

21039

NATIONAL LIBRARY
OTTAWA



BIBLIOTHÈQUE NATIONALE
OTTAWA

NAME OF AUTHOR..... ANIL KAPOOR

TITLE OF THESIS..... Lattice Thermal Conductivity
of Noble Metal Alloys

UNIVERSITY..... Univ of Alberta

DEGREE FOR WHICH THESIS WAS PRESENTED..... Ph D

YEAR THIS DEGREE GRANTED..... 1974

Permission is hereby granted to THE NATIONAL LIBRARY
OF CANADA to microfilm this thesis and to lend or sell copies
of the film.

The author reserves other publication rights, and
neither the thesis nor extensive extracts from it may be
printed or otherwise reproduced without the author's
written permission.

(Signed)..... Anil Kapoor

PERMANENT ADDRESS:
..... 4019-135 Ave
..... EDMONTON

DATED..... May 2nd 1974

THE UNIVERSITY OF ALBERTA

LATTICE THERMAL CONDUCTIVITY OF NOBLE METAL ALLOYS

by

© ANIL KAPOOR

A THESIS

SUBMITTED TO THE FACULTY OF GRADUATE STUDIES AND RESEARCH
IN PARTIAL FULFILLMENT OF THE REQUIREMENTS FOR THE DEGREE
OF DOCTOR OF PHILOSOPHY

IN

PHYSICS

DEPARTMENT OF PHYSICS

EDMONTON, ALBERTA

SPRING, 1974

THE UNIVERSITY OF ALBERTA

FACULTY OF GRADUATE STUDIES AND RESEARCH

The undersigned certify that they have read, and recommend to the Faculty of Graduate Studies and Research, for acceptance, a thesis entitled LATTICE THERMAL CONDUCTIVITY OF NOBLE METAL ALLOYS submitted by Anil Kapoor in partial fulfillment of the requirements for the degree of Doctor of Philosophy in Physics.

S. Rogers for S.B.W.
.....
Supervisor

John Turner
.....

F. Citron
.....

B. Parvatham
.....

H. Smith
.....
External Examiner

Date *April 29th 1974*
.....

TO MY LOVING PARENTS

ABSTRACT

Thermal conductivity measurements were made for two copper, two gold and one silver-based polycrystalline rods and one copper-based single crystal rod in the temperature range 0.5 to 4 K. The polycrystalline rods were measured with each rod first being in a highly cold-worked condition and then in various stages of recovery brought about by annealing at temperatures up to 1000 K. From the total measured conductivity the lattice conductivity was extracted by calculating the electronic component using the Wiedemann-Franz law and electrical resistivity measurements. In none of the alloys did the lattice conductivity exhibit the temperature dependence expected from standard theory. Above 1.5 K, comparable experimental results of other workers, published only for copper alloys, agreed with the data presented here. Measurements below 1.5 K indicated an even larger departure from standard theory. It is the author's belief, that in the entire temperature region (0.5 to 4 K), the anomalies are contained in that part of the lattice conductivity which is limited by defect scattering. The anomalies in the silver and gold alloys, though basically similar to those in copper alloys, occurred at different temperatures and could be due to changes in the scattering of phonons by dislocations,

with an associated "characteristic" length of a few hundred angstroms. Changes in the temperatures of the anomalies were correlated with changes in phonon wavelength in different hosts. A preliminary electron microscope investigation of the copper alloys reported here does indicate the presence of a "characteristic" length, of a few hundred angstroms, though not associated with the dislocation structure.

ACKNOWLEDGEMENTS

I wish to express my gratitude to the people without whom this thesis might not have been possible. — Professor S.B. Woods, my research supervisor, for suggesting this project and for his patience, understanding and guidance throughout; Dr. P.S. Turner and Mr. J.A. Brunel for the electron microscope work; Mr. D. Gerritsen for technical help and a special word of thanks to Dr. J.A. Rowlands for numerous valuable discussions and constant encouragement.

Finally, I would also like to thank my wife-to-be Wicki whose moral support was invaluable in completing this thesis.

TABLE OF CONTENTS

	<u>Page</u>
CHAPTER I INTRODUCTION *	1
CHAPTER II THEORETICAL BACKGROUND	3
2.1 Introduction	3
2.2 Separation of λ into Components	3
2.2.1 Electronic thermal resistivity	4
2.2.2 Lattice thermal resistivity	5
2.2.3 Graphical method of separation	7
2.3 Previous Work	7
2.4 Review of Models	8
2.4.1 Scattering of phonons by electrons	8
2.4.2 Scattering of phonons by static dislocations	9
2.4.3 Scattering of phonons by mobile dislocations	11
2.5 Need for Further Work	13
CHAPTER III EXPERIMENTAL DETAILS	14
3.1 Low Temperature Section	14
3.2 Temperature Controller	18
3.3 Thermometry	19
3.3.1 Choice of thermometers	19
3.3.2 Vapour pressure thermometry	21
3.3.3 Paramagnetic thermometry	22
3.3.4 Calibration of thermometers	25

	<u>Page</u>
CHAPTER III (cont'd)	
3.4 Measurement of Thermal Conductivity	26
3.5 Measurement of Electrical Resistivity	28
3.6 Test of Apparatus	29
CHAPTER IV SPECIMENS AND THEIR PREPARATION	34
4.1 Choice of Specimens	34
4.2 Specimen Preparation	34
4.2.1 Cu-10 at. % Al	35
4.2.2 Cu-30 at. % Zn	35
4.2.3 Cu-50 at. % Zn single crystal	37
4.2.4 Ag-2.1 at. % Al	37
4.2.5 Other alloys	37
4.2.6 Palladium	37
4.3 Annealing	38
CHAPTER V EXPERIMENTAL RESULTS	39
5.1 Graphical Presentation of Results	39
5.2 Copper Alloys	39
5.3 Silver and Gold Alloys	40
CHAPTER VI DISCUSSION OF MODELS AND EXPERIMENTAL RESULTS	64
6.1 Copper Alloys	64
6.1.1 Scattering of phonons by electrons or defects?	65
6.1.2 Estimates of electron limited lattice conductivity	67
6.1.3 Brass single crystal	69

	<u>Page</u>
CHAPTER VI (cont'd)	
6.2 Existing Models	69
6.2.1 Static dislocations	70
6.2.2 Mobile dislocations	71
6.2.3 Summary	74
6.3 Silver and Gold Alloys	75
6.4 "Effective" Phonon Wavelengths	77
CHAPTER VII SUGGESTIONS FOR FURTHER WORK	79
7.1 Superconductors	79
7.2 Electron Microscopy	80
7.3 Amorphous Materials	82
CHAPTER VIII CONCLUSIONS	85
BIBLIOGRAPHY	87
APPENDIX I	90
APPENDIX II	92

LIST OF TABLES

<u>Table</u>	<u>Description</u>	<u>Page</u>
1	Details of specimen	33
2	λ as a function of T for pure palladium	36
3	λ and λ_g as a function of T for <u>Cu-Al</u> (cold-worked)	43
4	λ and λ_g as a function of T for <u>Cu-Al</u> (annealed 600 K)	44
5	λ and λ_g as a function of T for <u>Cu-Al</u> (annealed 675 K)	45
6	λ and λ_g as a function of T for <u>Cu-Al</u> (annealed 1000 K)	46
7	λ and λ_g as a function of T for <u>Cu-Zn</u> (cold-worked)	48
8	λ and λ_g as a function of T for <u>Cu-Zn</u> (annealed 600 K)	49
9	λ and λ_g as a function of T for <u>Cu-Zn</u> (annealed 700 K)	50
10	λ and λ_g as a function of T for <u>Cu-Zn</u> (annealed 1000 K)	51
11	λ and λ_g as a function of T for <u>Cu-Zn</u> single crystal	53
12	λ and λ_g as a function of T for <u>Ag-Al</u> (cold-worked)	55
13	λ and λ_g as a function of T for <u>Ag-Al</u> (annealed 1000 K)	56
14	λ and λ_g as a function of T for <u>Au-Pt</u> (cold-worked)	58
15	λ and λ_g as a function of T for <u>Au-Pt</u> (annealed and then rolled)	59
16	λ and λ_g as a function of T for <u>Au-Pt</u> (annealed 1000 K)	60

<u>Table</u>	<u>Description</u>	<u>Page</u>
17	λ and λ_g as a function of T for <u>Au-Ag</u> (cold-worked)	62
18	λ and λ_g as a function of T for <u>Au-Ag</u> (annealed 1000 K)	63
19	Effective phonon wavelengths at T_B	78

LIST OF FIGURES

<u>Figure</u>	<u>Description</u>	<u>Page</u>
1	Low temperature section of cryostat	15
2	$\lambda\rho/T$ vs T^2 for pure palladium	31
3	$\lambda\rho/T$ vs T for pure palladium	32
4	λ/T vs T for <u>Cu-10</u> at. % Al	42
5	λ/T vs T for <u>Cu-30</u> at. % Zn	47
6	λ/T vs T for <u>Cu-30</u> at. % Zn single crystal	52
7	λ/T vs T for <u>Ag-2.1</u> at. % Al	54
8	λ/T vs T for <u>Au-2</u> at. % Pt	57
9	λ/T vs T for <u>Au-10</u> at. % Ag	61
10	$W_g T^2$ vs concentration for <u>Cu-Zn</u> alloys	68
11	Electron micrographs of <u>Cu-Al</u> and <u>Cu-Zn</u>	81
12	λ_g vs T for <u>Cu-Al</u> and some amorphous materials	84
13	Universal plots	93

INTRODUCTION

Thermal conductivity measurements of some cold-worked copper alloys have been reported recently by Kusonoki and Suzuki (1969), Charsley and co-workers (1968, 1971) and Mitchell et al (1971). These measurements indicate that the lattice thermal conductivity does not follow the expected quadratic temperature dependence in the range 1.5 to 4 K. Although the experimental results, of the above workers, were basically similar, various explanations have been put forward for the anomalous behaviour of the lattice conductivity. These anomalies have been attributed to: (a) a change in the electron-phonon interaction due to short electron mean free paths (Lindenfeld and Pennebaker 1962) or (b) a change in the scattering of phonons by (i) static dislocations and (ii) mobile dislocations. This thesis is an attempt to resolve the controversy by extending the measurements to lower temperatures (0.5 K) and to other noble metal hosts (silver and gold).

The various components of thermal conductivity are discussed in Chapter II along with a review of the previous work and proposed models. A description of the ^3He cryostat, used for the measurements reported here, along with experimental details are given in Chapter III. Chapter IV is concerned with the choice

and preparation of specimens and all the thermal conductivity results are presented in Chapter V. A discussion of results with reference to various models follows in Chapter VI. Some suggestions for further work have been put forward in Chapter VII. The final chapter is a summary of the conclusions.

CHAPTER II

THEORETICAL BACKGROUND

2.1 Introduction

The thermal conductivity λ of a metal may be divided into two components, the electronic conductivity, λ_e , and the lattice conductivity, λ_g . This thesis is primarily concerned with the measurement and analysis of the lattice thermal conductivity of metal alloys, at low temperatures. In a pure metal most of the heat is transported by the electrons and consequently it is extremely difficult to measure λ_g . Point imperfections added to the host metal reduce the electronic component without substantially reducing the lattice component at low temperatures. The two components, λ_e and λ_g , are then comparable and λ_g becomes a measurable quantity.

2.2 Separation of λ into Components

The total thermal conductivity λ can be written as a sum of its electronic and lattice components (Klemens 1958), so that

$$\lambda = \lambda_e + \lambda_g \quad (2.1)$$

These two conduction processes are limited by various

scattering mechanisms that give rise to thermal resistances $W_e = \lambda_e^{-1}$ and $W_g = \lambda_g^{-1}$. It is then necessary to consider the various mechanisms that will scatter the electrons and phonons to arrive at the total thermal resistivity, and hence the total thermal conductivity. The electronic thermal resistivity is discussed in the next section and the lattice thermal resistivity is discussed in Sec. 2.2.2.

2.2.1 Electronic Thermal Resistivity

There are two major sources of electron scattering in alloys: imperfections and lattice vibrations. These give rise to thermal resistivities W_{eo} and W_{ei} where the subscript o denotes the imperfection induced (or residual) resistivity, and the subscript i the ideal (or lattice) resistivity. Below 4 K, the alloys reported here have a negligible W_{ei} because $W_{eo} \gg W_{ei}$. The electronic thermal conductivity is then given by the Wiedemann-Franz law (Klemens 1958).

$$\lambda_e = L_o T / \rho_o \quad (2.2)$$

where ρ_o is the residual electrical resistivity and L_o is the classical Lorenz number = $2.445 \times 10^{-8} \text{ W}\Omega\text{K}^{-2}$.

2.2.2 Lattice Thermal Resistivity

The various scattering mechanisms for phonons are

- 1) specimen boundaries
- 2) electrons
- 3) dislocations
- 4) point defects and δ
- 5) interaction with other phonons.

The important sources of lattice resistivity in the alloys reported here, below 4 K, are electrons, W_{ge} , and the strain fields surrounding dislocations, W_{gd} . A physically plausible argument is presented below to show why W_{ge} has T^{-2} temperature dependence.

Using the dominant phonon approximation (Ziman 1958) one can write

$$\lambda_g \propto C_g v \ell \tag{2.3}$$

where C_g represents the lattice specific heat, ℓ the mean free path of phonons and v the velocity of these phonons. Below 4 K, v can be assumed to be independent of temperature and $C_g \propto T^3$, so that only the temperature dependence of ℓ remains to be determined. The phonons can interact only with those electrons within the "thermal layer" around the Fermi surface. Since the "thermal layer" is $\sim kT$ in width, the number of electrons

available for scattering is proportional to T , so that $\lambda \propto 1/T$. Using eqn. (2.3), $W_{ge} \propto T^{-2}$ is obtained.

This temperature dependence was experimentally verified by White and Woods (1954), Kemp et al (1957), White, Woods and Elford (1959) and Birch et al (1959), who deduced λ_{ge} in pure copper, silver and gold from measurements of the thermal conductivity of dilute alloys.

Klemens (1958) has shown that the lattice thermal resistivity arising from the scattering of phonons by dislocations also varies as T^{-2} . In his calculation, scattering by the dislocation core is shown to be negligible at low temperatures, the majority of the scattering being due to the long range strain field. In the range 4-20 K, thermal resistances varying as T^{-2} have been experimentally observed by Birch et al (1959), in alloys where a high density of dislocations had been introduced.

Since both W_{ge} and W_{gd} arise from phonon processes with the same frequency dependence, it can be assumed that they contribute additively to W_g (Klemens 1958), so that

$$W_g = W_{ge} + W_{gd} \quad (2.4)$$

or

$$W_g = CT^{-2} + DT^{-2} \quad (2.5)$$

The calculation of the total thermal resistivity for scattering processes of different frequency dependences is discussed in Appendix II.

2.2.3 Graphical Method of Separation

Using eqns. (2.1) and (2.2) the total conductivity λ can be written as

$$\lambda = L_0 T / \rho_0 + BT^2 \quad (2.6)$$

where

$$B \equiv C + D$$

Plots of λ/T against T would thus be expected to give a straight line with intercept L_0/ρ_0 and slope B which will depend on the density of dislocations.

2.3 Previous Work

Mitchell et al (1971), Leaver and Charsley (1971) and Kusonoki and Suzuki (1969) made independent studies of λ_g , in the temperature range 1.5 to 4 K, on deformed and subsequently annealed copper alloys containing between 2 and 15 at. % aluminum. The thermal conductivity data measured by all three groups of workers was basically similar and showed a pronounced change in temperature dependence, or "kink", between 2 and 3 K. Although the three groups attributed this change to an effect in the lattice thermal conductivity, each advanced a different explanation for it. The models they used are briefly discussed in the next section.

2.4 Review of Models

The various models suggested can be discussed in three categories:-

- (1) Scattering of phonons by electrons (in the region where the electronic mean free path = phonon wavelength) - Pippard effect (1957).
- (2) Scattering of phonons by static dislocations
 - (a) Dislocation 'dipole' model by Leaver and Charsley (1971).
 - (b) Dislocation rearrangement model of Ackerman and Klemens (1971).
- (3) Scattering of phonons by mobile dislocations
 - (a) Dislocation 'flutter' model as discussed by Ziman (1960).
 - (b) Resonance scattering by partial dislocations - Kronmüller (1972).

2.4.1 Scattering of Phonons by Electrons

Pippard (1957) has shown that the electron-limited lattice thermal conductivity will depart from the usual T^2 dependence when $q\ell_e \leq 1$ where q represents the phonon wave vector and ℓ_e the electronic mean free path). The inequality $q\ell_e < 1$ implies that the electrons do not travel sufficiently far between scattering events to 'sample' one complete wavelength of the

lattice vibration. The interaction between phonons and electrons is thereby reduced and leads to an extra lattice conductivity proportional to T . Experiments by Zimmerman (1959) and Jericho (1965) on silver alloys, by Lindenfeld (1962) on copper alloys and by Archibald et al (1967) on potassium alloys (of comparable ρ_0), do show an increase in the thermal conductivity below 2-3 K. Mitchell et al (1971) have interpreted their data, on cold worked and annealed copper alloys, also in support of Pippard's theory.

2.4.2 Scattering of Phonons by Static Dislocations

(a) Dislocation 'dipole' model

The scattering of phonons by the long range strain field of dislocations produces a T^2 variation of λ_g at low temperatures. However, the probability that a phonon will be scattered by a defect depends on the relative size of the defect and the phonon wavelength. As the temperature decreases the dominant phonon wavelength increases and the phonon scattering begins to be affected by the overlap of some of the dislocation strain fields. This overlap leads to a reduction in the scattering, as, on the average, the strain fields tend to cancel each other.

In the Leaver and Charsley (1971) model a fraction of the dislocations are assumed to be in a 'dipole'

arrangement. In the dipole configuration, two parallel edge dislocations of opposite signs are separated by distances small compared with other dislocation separations. Since the long range strain fields of the two dislocations in such an arrangement partially cancel, one expects a decrease in phonon scattering compared to that of two isolated dislocations. Leaver and Charsley (1971) assumed that dislocation dipoles would scatter phonons, which have a wavelength greater than n times the dipole separation, with $\ell \propto \omega^{-3}$ (n is an adjustable parameter and ω is the phonon frequency). All other phonons would be scattered as for an individual dislocation, i.e. $\ell \propto \omega^{-1}$ (Gruner and Bross 1968).

Choosing values of $d \approx 200-250 \text{ \AA}$ (from electron microscope data), n was varied to optimize the fit to the data. For $d = 250 \text{ \AA}$ and $n = 0.5$, Leaver and Charsley found good agreement with experimental curves in the temperature range 2 to 4 K. Their calculations of λ_g below 2 K showed a plateau in λ_g/T against T plots around 1 K.

(b) Dislocation arrangement model

Ackerman and Klemens (1971) calculated the lattice thermal conductivity due to a dense array of dislocations. On the assumption that dislocations tend to rearrange themselves so as to minimize the free energy, they showed that this leads to a cancellation of the long range

strain field. This model though similar to the Leaver and Charsley model, is much less restrictive on dislocation arrangements and would lead to a slower deviation from a T^2 behaviour than the 'dipole' model.

2.4.3 Scattering of Phonons by Mobile Dislocations

(a) Dislocation-flutter model

So far the dislocation and its surrounding strain field have been treated as static entities. However, it is known that dislocations are not fixed to the medium but can move. This mobility should be taken into account in the analysis of scattering, for the incident phonon has a stress field which may cause the dislocation to move while scattering the incident phonon. Ziman (1960) has shown that the scattering width is proportional to the phonon wavelength, so that

$$W_{gd} \propto T^{-4}$$

To date, the only experiments which indicate such a strong temperature dependence of λ_g are measurements made by Jericho (1965) and Lindenfeld (1966).

(b) Resonance scattering by partial dislocations

In a face-centred cubic metal a dislocation may dissociate into two partial dislocations, separated by a stacking fault - a region across which the sequence

of close-packed layers is disturbed. Kronmüller (1972) has calculated the vibrational frequencies of these partial dislocations to be 10^{10} to 10^{11} Hz which correspond to the dominant phonon frequencies at 1 K. Resonant scattering of phonons by vibrating partials can, therefore, produce a change in the phonon conductivity close to 1 K. The resonant frequency ω_0 is directly proportional to the stacking fault energy, and inversely to the stacking fault width (Kronmüller 1972) so that:

$$\omega_0 = (2\gamma/m_{\text{eff}}d)^{1/2} \quad (2.7)$$

where

$\gamma \equiv$ stacking fault energy

$d \equiv$ stacking fault width

$m_{\text{eff}} \equiv$ effective dislocation mass .

At resonance, the scattering of phonons would be enhanced and this would lead to a plateau in the lattice conductivity or, under special circumstances, a minimum. Thermal conductivity measurements on superconducting niobium single crystals have been interpreted by Anderson and Smith (1973) as indicating a resonant scattering of phonons around 1 K.

2.5 Need for Further Work

As various explanations existed for the anomalous behaviour of the lattice thermal conductivity of cold worked copper alloys, it was anticipated that extending the measurements down to liquid ^3He temperatures would clarify the situation. Preliminary measurements on copper alloys, of the same type studied by others, yielded similar experimental data in the liquid ^4He region, and enhanced conductivities in the ^3He region. It seemed that measurements on other, cold-worked, noble metal hosts (where the phonon wavelengths were different) would be helpful.

CHAPTER III

EXPERIMENTAL DETAILS

In order to measure the thermal conductivity of various metals and alloys, in the temperature range 0.5-4 K, a ^3He cryostat was constructed. The design of the cryostat was similar to the one described by Archibald, Dunick and Jericho (1967), with a few modifications. Both the thermal conductivity and the electrical resistivity of a specimen can be measured, over the entire temperature range, in a single run.

3.1 Low Temperature Section

At all temperatures the main coolant is liquid ^4He in a glass dewar, boiling under normal pressure. For measurements between 2 and 4 K, liquid ^4He in a thermally isolated copper pot is cooled by reducing the pressure above it. For measurements below 2 K, a further stage of refrigeration is used; a pumped pot containing liquid ^3He .

A cross-section of the low temperature part of the cryostat is shown in Fig. 1. It consists of three main sections:

- (i) a copper outer can,
 - (ii) the ^4He pot with an isothermal radiation shield,
- and

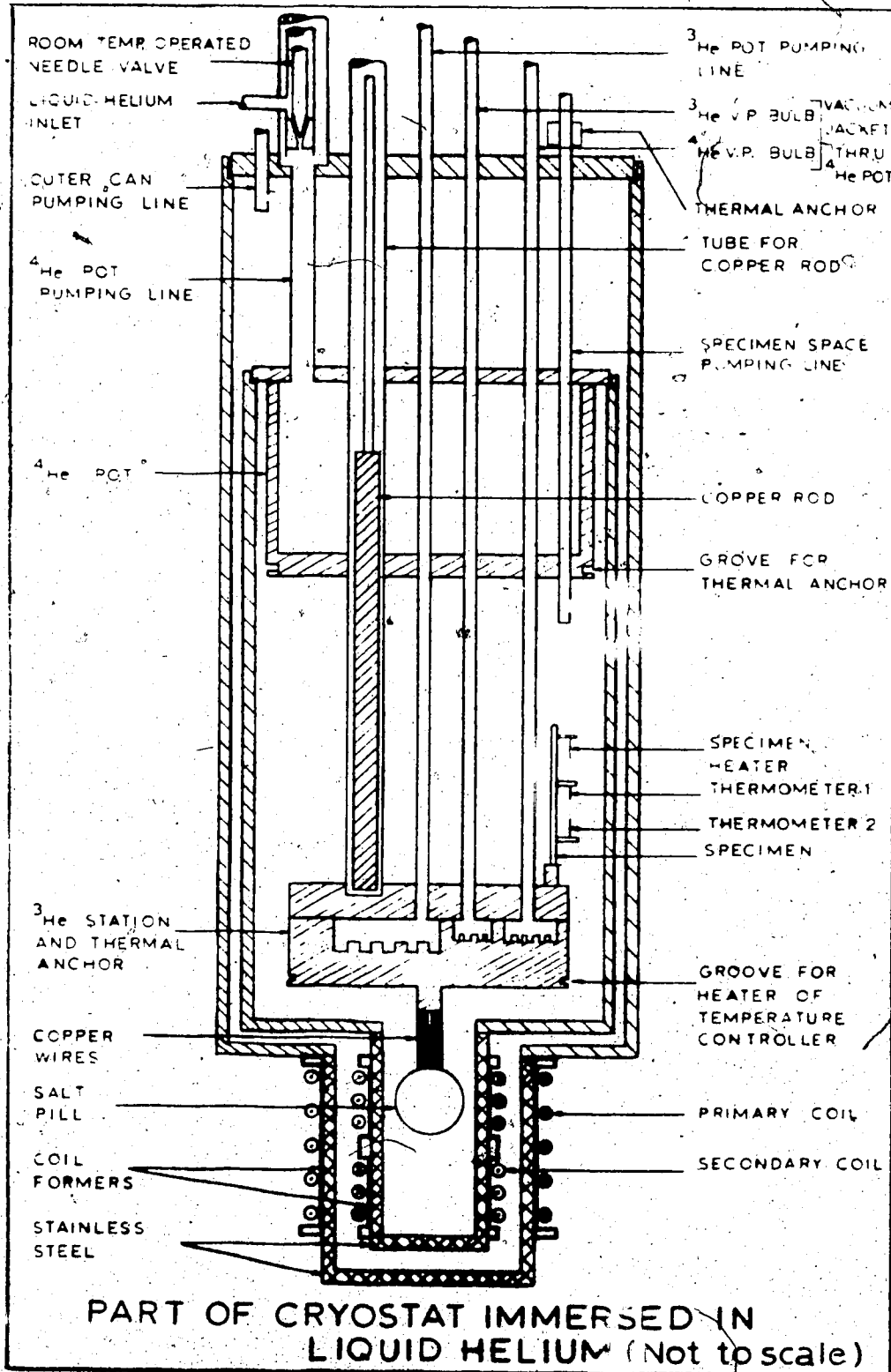


Fig. 1. The Cryostat.

(iii) the ^3He station to which the specimen is soldered.

The outer can, cooled by immersion in a dewar of liquid ^4He , can be evacuated, thereby isolating the ^4He station. The ^4He pot (a 150 c.c. copper pot) can be filled with liquid ^4He and pumped to obtain temperatures between 1.2 and 4 K. Extending below the pot is a removable, brass inner can (enclosing the ^3He station) which can be evacuated by a separate pumping system. The ^3He station, a copper block with various chambers machined into it, is comprised of the following:

- (i) a ^3He pot of capacity 3 c.c. which can be pumped to obtain temperatures down to 0.4 K,
- (ii) ^4He and ^3He vapour pressure bulbs,
- (iii) a specimen post,
- (iv) carbon resistors and a heater used for temperature regulation,
- (v) a salt pill, hung directly below the ^3He station and isothermal with it.

Starting at the room temperature cryostat head, the electrical leads, including spares, pass down the specimen chamber pumping tube. The lower end of this tube passes through a brass block as shown in Fig. 1. The wires were wrapped around and varnished to a copper post, which was then soldered with Wood's alloy into the brass block. This block was normally covered with liquid ^4He thus providing the first thermal

anchoring stage for the wires. The leads were again thermally anchored at the ^4He pot and ^3He station as indicated in Fig. 1. To keep the heat leak to the two stations small, #38 B & S manganin wire was used for all leads except the single current lead, for which #38 B & S copper wire was used. The free ends of the leads at the ^3He station were soldered to electrically insulated pins embedded in a copper post. Electrical connections to the specimen, thermometers and heaters were made with coils of manganin wire, eight inches long ($70 \Omega/\text{ft}$), ensuring that the thermal resistance in parallel with the specimen was large enough to prevent the heat flow through it from being disturbed.

The procedure used in cooling the cryostat was to introduce exchange gas (^4He) at a pressure of several Torr into the outer and inner cans. Liquid nitrogen was used for pre-cooling. The dewar was then emptied and liquid ^4He was then transferred into it, cooling the whole low temperature section (Fig. 1) to 4 K. The exchange gas was pumped out and the ^4He pot filled with liquid through the needle valve, operated from the cryostat head at room temperature. The ^4He pot and the ^3He station were kept in thermal contact by lowering the movable copper rod and filling the tube around it with ^4He gas at a pressure of several Torr. Temperatures between 2 and 4 K were obtained by pumping

the ^4He pot, controlling the pressure with a diaphragm manostat, and supplying a small amount of heat through the temperature controller. For measurements at lower temperatures the ^3He pot was filled with liquid by introducing ^3He at a pressure of about 250 Torr. The thermal linkage between the ^3He and ^4He stations was then "broken" and the ^3He pot pumped through a room temperature needle valve to slightly below the required temperature. The temperature was regulated at a slightly higher value with a heater connected to a temperature controller.

3.2 Temperature Controller

The temperature controller is similar to the one described by Rochlin (1970). The circuit consists of an a.c. wheatstone bridge with a carbon resistance thermometer, as the sensing element, in one arm of the bridge. Regulation is provided by using the off-null signal, amplified by a phase sensitive detector, to control the power delivered to a heater placed in good thermal contact with the ^3He station. This 1000 Ω heater, consisting of #42 B & S manganin wire (147 Ω/ft), was wound around the ^3He station as shown in Fig. 1. Since the bridge was optimized for thermometer resistances between 500 and 5000 Ω it was necessary to use

12

two different thermometers to cover the entire temperature range (a 33 Ω Allen Bradley from 1.5 to 4 K and a 10 Ω one below 1.5 K). The resulting regulation of the ^3He station temperature was better than ± 0.5 mK.

3.3 Thermometry

3.3.1 Choice of Thermometers

A pair of fast responding thermometers are required for thermal conductivity measurements. The possible choices are carbon or germanium resistance thermometers. The advantages of using carbon resistors are (i) they are cheap and (ii) their resistance-temperature characteristics can be fitted to a simple equation. The disadvantage is that they have to be recalibrated every run. In contrast, germanium thermometers are more expensive, fit a more elaborate equation, but once calibrated hold their calibration well. This excellent reproducibility was the major reason we chose to use germanium thermometers. The thermometers were calibrated in the cryostat, as described later, and checked periodically.

It is important not to use too large a measuring current to avoid self-heating of the thermometers. Test experiments showed that at 10 μA no change in temperature occurred even at 0.5 K. Consequently, this

current was used for measuring the thermometer resistances at all temperatures. At all temperatures changes in thermometer resistance corresponding to temperature changes of 0.1 mK could be easily detected.

At temperatures below 1 K extreme care has to be taken to ensure good thermal contact between the thermometer and the specimen. Below 1 K the pressure of the exchange gas in the thermometer capsule drops resulting in the temperature of the sensing element being different from the temperature of the thermometer casing. To circumvent this problem the specimen probe was thermally anchored to the thermometer leads as well as the thermometer case. A piece of #18 B & S gauge enamelled copper wire was wrapped around the case of the thermometer in a single layer and varnished. One end of the wire was soldered to the specimen probe using non-superconducting solder (bismuth-cadmium). The other end of the wire was used as a thermal anchor for the thermometer leads by winding and varnishing them to it.

The probes themselves were 2 cm long pieces of #14 B & S gauge bare copper wire, wrapped around the specimen in a single turn, transverse to the specimen axis, and soldered with non-superconducting solder. Initially a different method was tried. A 1 mm diam. copper wire was etched carefully in concentrated acid

into a conical shape. Holes were drilled, in the specimen, at two convenient points (about 8 cm apart) and the thin end of the etched wire drawn through until it fit snugly. This would have allowed the probes to be left in place between runs, whilst the specimen was annealed, ensuring that the separation of the probes remained constant. This procedure was unsuccessful as below 1 K the pressure contact had too high a thermal resistance.

3.3.2 Vapour-Pressure Thermometry

The pressures of ^4He and ^3He in the vapour pressure bulbs were measured using two precision pressure gauges manufactured by Texas Instruments. These gauges have a high sensitivity and reproducibility (± 0.001 Torr.). Between 2 and 4 K temperature measurements were made by reading the vapour pressure of ^4He and using the T^{58} scale (Brickwedde et al 1960). In order to prevent errors due to cold spots the vapour pressure sensing tubes were vacuum jacketed where they passed through the ^4He pot. Below 2 K, the ^4He bulb was evacuated and temperatures were obtained from ^3He vapour pressure measurements using the T^{62} scale (Sherman, Sydoriak and Roberts 1964). In the overlap region, between 2 and 3 K, the pressures over the two

bulbs were read simultaneously and the corresponding temperatures were found to be the same within ± 0.1 mK.

Below 0.7 K thermomolecular pressure corrections, which are difficult to estimate accurately, have to be applied, so the range for ^3He vapour pressure measurements was limited to 0.7 to 2 K. Using this combination, the T^{58} scale for ^4He and the T^{62} scale for ^3He , temperatures were reproduced over the range 0.7 to 4 K with an accuracy of ± 0.1 mK.

3.3.3 Paramagnetic Thermometry

Paramagnetic thermometry is based on the temperature dependence of susceptibility of an almost non-interacting system of spins. The general equation governing their behaviour is the Curie-Weiss law

$$\chi = \frac{C}{T - \theta} \quad (3.1)$$

where

C = Curie constant,

T = Temperature,

θ = Weiss constant, and

χ = Susceptibility.

Three different salts were tried in turn:

(a) Cerium Magnesium Nitrate (CMN),

- (b) Ferric Ammonium Alum,
- (c) Potassium Chrome Alum.

CMN is known to obey Curie's law down to ~ 0.01 K and probably somewhat below (Abel et al 1964). However, fairly sensitive methods of measurement are required because the material has a small Curie constant. Ferric ammonium alum was therefore tried as it has a large Curie constant. However, the salt is extremely unstable since it loses its water of hydration very easily. Finally, potassium chrome alum was tried.

The thermal and magnetic properties of potassium chrome alum are fairly well known below 1 K (Bleaney 1950, Daniels and Kurti 1954). The salt was used in the form of a sphere $7/8$ inch in diameter. The ends of about 300 strands of enamelled #38 B & S gauge copper wire were embedded in the sphere to provide thermal contact with the ^3He station as shown in Fig. 1. The salt and an epoxy mixture (Harrison 1968) were cast in a split teflon mould with a hole for the sheaf of wires. The exposed ends of the wires were then soldered to the specimen station about 2 inches from the salt sphere.

The susceptibility of the salt, as a function of temperature, was determined from the change in mutual inductance of a pair of concentric coils which surrounded the salt. Mutual inductance measurements were made using a 17 Hz inductance bridge (Pillinger, Jastrum and

Daunt 1958). The primary coil consists of 3000 turns of #38 B & S gauge enamelled copper wire wound on a teflon former which fitted closely over the narrow end (tail) of the outer can. Both the outer can and the inner can had tails (as shown in Fig. 1) made from non-magnetic stainless steel tubing. The secondary coil, mounted on the tail of the inner can, was wound in two sections on a single former. Each section consisted of 4000 turns of #40 B & S gauge enamelled copper wire, wound in opposition and connected to reduce the total mutual inductance to as small a value as possible. Copper leads were used to make connections between the two coils and the mutual inductance bridge. A few extra turns on one half of the secondary or slight misalignment on assembly or cooling, made a considerable difference to the total mutual inductance of the coils which could result in the mutual inductance lying outside the range of the bridge. Consequently the range of the bridge was extended by a factor of ten by replacing the standard 5 mH plate coil in the bridge by a "home-made" mutual inductor of value about 500 mH.

To determine M_0 , (the mutual inductance in the absence of the salt pill) the measured mutual inductance M for the system with salt pill in place is first plotted as a function of $1/T$ (T from 0.7 to 2 K) and

this curve extrapolated to $T = \infty$ gives M_0 . Then $M - M_0$ is proportional to the temperature dependent part of the susceptibility of the salt.

Since vapour pressure measurements were used to determine the absolute temperature T from 0.7 to 4 K, it was only in the range 0.4 to 0.7 K that the magnetic temperature T^* had to be converted to the absolute temperature T . However, in this temperature region, the difference between T and T^* for Potassium Chrome Alum is negligible (Cooke 1949).

3.3.4 Calibration of Thermometers

The thermometers were calibrated by mounting them on a specimen of high thermal conductivity, soldered to the ^3He station. Fifty different temperatures of this station were maintained and measured as described earlier. The resistances of the two germanium thermometers were measured, in rapid sequence, at each temperature. The data were then fitted to an equation of the form used by Blakemore (1970).

$$\ln R = \sum_{i=0}^n A_i (\ln T)^i \quad (3.2)$$

Chebyshev polynomials and double precision were used for sufficient accuracy and it was found that a value of $n = 7$ gave the best fit. A deviation curve of

$(T_{\text{cal}} - T_{\text{exp}})$ vs T_{exp} was plotted, where T_{cal} were the calculated temperatures using eqn. (3.2) and T_{exp} were the experimental temperatures. Since the deviation curves for the two thermometers were very similar the corrections applied were generally less than 1 mK. A table of R vs T at intervals of 0.1 mK was generated for each thermometer, so that thermal conductivity calculations could be made quickly while a run was in progress.

3.4 Measurement of Thermal Conductivity

Measurements of the thermal conductivity $\lambda(T)$ were made in the steady state by passing a constant heat current Q down the specimen and measuring the temperature difference ΔT between two points. Then:

$$\lambda(T) = Q(\ell/a)/\Delta T \quad (3.3)$$

where ℓ is the length between thermometer connections and A is the cross-sectional area of the specimen.

Current leads to the two germanium thermometers were connected in series. The specimen heater, of 1500 ohms resistance, was made by winding #40 B & S gauge manganin wire on a 2 mm diameter insulated copper wire. This was attached to the specimen with Wood's alloy. Current leads to the heater from the ^3He station were

superconducting (lead plated manganin wire), thus eliminating any corrections due to joule heating in them.

To measure the thermal conductivity at any given temperature T , the ^3He station was first stabilized at a temperature slightly below T . The specimen heater was switched on and the power adjusted to produce a reasonable ΔT . Generally ΔT was ≈ 150 mK at 4 K and ≈ 40 mK at 0.5 K. Both thermometers were read in rapid sequence and their temperatures recorded when they became steady. The heater was then switched off and the two temperatures recorded again in the steady state with $Q = 0$. This procedure was repeated twice to ensure that there was no appreciable drift in the temperature of the ^3He station. Then

$$\Delta T = (\Delta T)_2 - (\Delta T)_1, \quad \text{where}$$

$(\Delta T)_2$ is the difference between the upper thermometer readings with the heater ON and OFF, and

$(\Delta T)_1$ is the difference between the lower thermometer readings with the heater ON and off.

The temperature T is the mean temperature $(T_1 + T_2)/2$, where T_2 and T_1 are the temperatures of the upper and lower thermometers respectively with the specimen heater ON.

The heat Q , produced by the heater, is determined by measuring the current I through and the potential V across the heater with a potentiometer. Then $Q = IV$. Measurement of the geometrical shape factor l/A allows eqn. (3.3) to be applied to obtain $\lambda(T)$.

3.5 Measurement of Electrical Resistivity

The electrical resistance of a specimen can be represented by

$$R = \rho \cdot (l/A)$$

where R is the electrical resistance, ρ the electrical resistivity and (l/A) the geometrical factor. Since the electrical resistance and thermal conductivity of a specimen are measured in the same run using the same probes the shape factor remains the same for both measurements.

The electrical resistance was measured by passing a constant current through the specimen and a standard resistor and comparing the voltage drop produced across each. A four-terminal potentiometric arrangement was used to measure these voltages and currents were reversed to eliminate thermo-electric voltages. All the specimens used had a resistance of $\approx 400 \mu\Omega$ so that a current of 50 ma produced a voltage drop of 20 μV across the specimen. Since the smallest

detectable voltage was 100 nanovolts (nV), the resistance of the specimen could be measured to an accuracy of $\frac{1}{2}$ %. Manganin wires were used for the two potential leads and current to the specimen was carried down a copper lead. The return path of the current was through the cryostat.

The resistance of a specimen was generally first measured by immersing the specimen directly in liquid helium, in a storage dewar. The specimen was then mounted in the cryostat and its resistance measured at 4 K with ^4He exchange gas present in the specimen chamber. For resistivity measurements below 1 K a different potentiometer was used with a galvanometer amplifier as the null detector. This increased the sensitivity and measurements could be made to the same accuracy using smaller currents.

3.6 Test of Apparatus

As a test of the apparatus, a test specimen with known conductivity and with a conductance similar to the alloys was required. Pure palladium (impurity content < 12 ppm) was chosen, since in a pure material

- (a) the lattice conductivity could be assumed to be negligible compared to the electronic conductivity and
- (b) the low temperature limiting value of the ideal scattering process for electronic conductivity was known

from the thorough work of Schriempf (1967, 1968).

The electrical resistivity of the specimen was measured over the entire temperature range, 0.5 to 4 K, and the data could be fitted by the expression

$$\rho = (6.01 + 0.003 T^2) \times 10^{-8} \text{ } \Omega \text{ cm},$$

which for the T^2 term is in good agreement with the data of Schriempf (1968) obtained above 2 K.

Schriempf's data (1967) can be expressed as $\lambda_p/T = L'_0 - BT^2$ where $L'_0 = 2.48 \times 10^{-8} \text{ W}\mu\text{K}^{-2}$ and B depends on ρ_0 . In Fig. 2, λ_p/T for the palladium specimen is plotted against T^2 and fitted by a least squares procedure, yielding $L'_0 = 2.48 \times 10^{-8} \text{ W}\mu\text{K}^{-2}$, which is identical to Schriempf's value.

In Fig. 3, λ_p/T is plotted against T to provide a comparison with the lots for the alloys discussed later. The value for L'_0 , obtained by fitting a straight line to this plot, is the same as that of Fig. 2, within experimental error, although the extrapolation may have no physical justification. However, the data points fit the line smoothly with small scatter and without any sign of the "bumps" or "kinks" that are apparent in most of the alloy data.

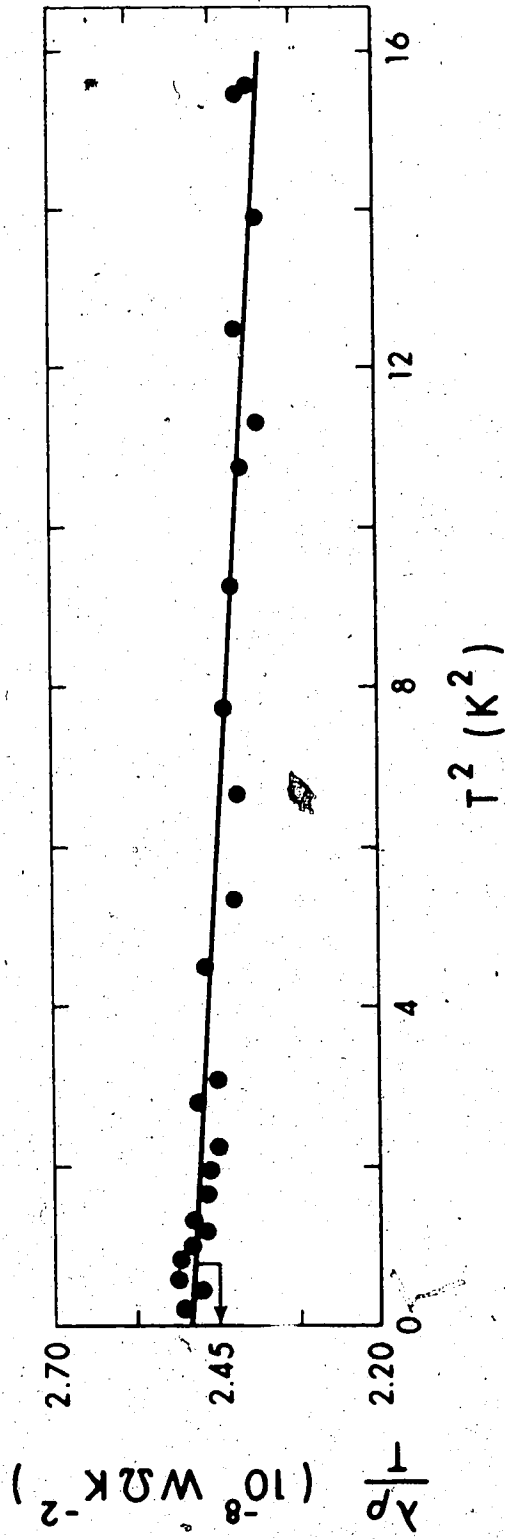


Fig. 2. Plot of the experimental Lorenz ratio against the square of the absolute temperature for the pure Pd specimen. The horizontal arrow indicates L_0 .

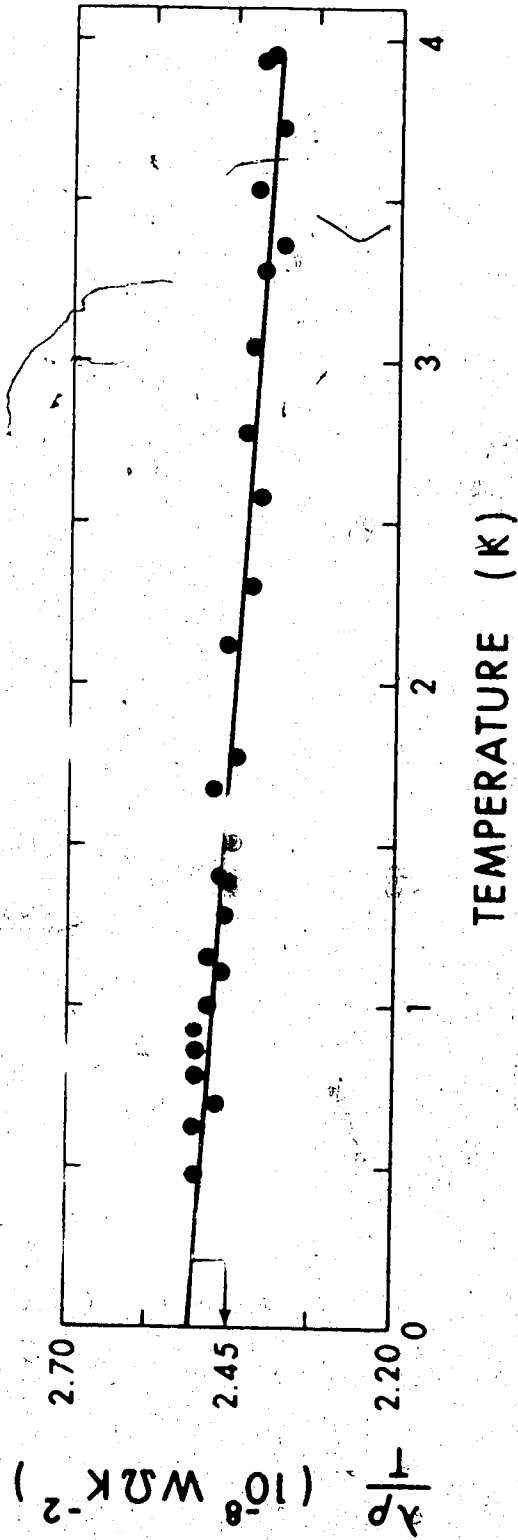


Fig. 3. Plot of the experimental Lorenz ratio against the absolute temperature for the pure Pd specimen. The horizontal arrow indicates L_0 .

Table 1

Total thermal conductivity λ in $\text{W cm}^{-1} \text{K}^{-1}$ as a function of temperature T in degrees K for pure palladium.

$$\rho_0 = 6.06 \times 10^{-8} \text{ } \Omega\text{-cm}$$

$$l/a = 6433 \text{ cm}^{-1}$$

T	λ	T	λ
3.946	1.557	1.509	0.612
3.933	1.560	1.405	0.576
3.726	1.462	1.395	0.568
3.534	1.409	1.283	0.523
3.362	1.320	1.154	0.476
3.282	1.304	1.104	0.451
3.043	1.217	1.005	0.412
2.779	1.118	0.935	0.388
2.584	1.030	0.865	0.360
2.306	0.925	0.787	0.327
2.121	0.865	0.699	0.287
1.755	0.711	0.630	0.262
1.676	0.688	0.483	0.201

CHAPTER IV

SPECIMENS AND THEIR PREPARATION

4.1 Choice of Specimens

The specimens used were fairly concentrated alloys in order to: (a) ensure that the electronic component of thermal conductivity was reduced, making it comparable with the lattice component and (b) make the total electrical resistivity practically temperature independent. The geometrical shape factor, l/a , of each specimen was chosen so that the thermal conductance $Q/\Delta T$ at 4 K was similar for all specimens. This required the resistance R of each specimen to be about $500 \mu\Omega$. Phase diagrams (Hansen 1958) were checked to ensure that all alloys were within the solid solution region.

4.2 Specimen Preparation

A general procedure for preparing the specimens is outlined below. The pure materials were lightly etched and weighed. They were then melted either under vacuum or argon in either quartz or recrystallized alumina crucibles using a R.F. induction furnace. The resulting ingots were swaged or rolled to produce a rod of the required dimensions. A list of the specimens,

along with their residual resistivities, and annealing temperatures, is given in Table 2.

4.2.1 Cu-10 at. % Al

This alloy was prepared by induction melting 99.999 % pure aluminum with OFHC copper in a 1/4" bore evacuated quartz tube. The resulting ingot was etched and then swaged in a number of stages, to 3.6 mm diameter. The specimen used was 10 cm long and was stored in liquid nitrogen to retain maximum cold-work.

4.2.2 Cu-30 at. % Zn

The boiling point of zinc (907°C) is much lower than the melting point of copper (1083°C). Consequently, in the process of melting in the induction furnace, a large proportion of the zinc was lost by evaporation. This problem was circumvented by starting with larger quantities. The copper was melted first and the zinc dissolved in it. Four cylindrical rods (1/2" diameter) 10" long were cast into sand moulds at the American Brass Foundries, Edmonton. One rod was swaged down to 3/8" diameter, annealed, and then swaged to 1/4" diameter. The intermediate anneal was necessary to prevent cracking. Specimens 12 cm long and 4 mm in diameter were machined from this material.

Table 2
 Details of Specimens

Specimen	Symbol	Residual Resistivity ($\mu\Omega\text{cm}$)	Annealing Temp. (K)
<u>Cu-10 % Al</u>			
cold-worked	●	7.54	
first anneal	□	6.79	600 K
second anneal	△	6.88	675 K
final anneal	○	6.69	1000 K
<u>Cu-30 % Zn (α-brass)</u>			
cold-worked	●	4.59	
first anneal	□	3.82	600 K
second anneal	△	3.77	700 K
final anneal	○	3.86	1000 K
Brass single crystal	●	3.53	
<u>Au-2 % Pt</u>			
cold-worked	●	1.84	
annealed	○	1.96	1000 K
<u>Au-10 % Ag</u>			
cold-worked	●	2.90	
annealed	○	2.71	1000 K
<u>Ag-2.1 % Al</u>			
cold-worked	●	3.43	
annealed	○	3.27	1000 K
Palladium	●	0.061	

4.2.3 Cu-30 at. % Zn Single Crystal

Two single crystals of brass were obtained from a commercial source (Windsor Metalcrystals 1973). One was a 1/2" diameter cylindrical rod and was spark cut into 1/8" square rods 6" long. The other, 1/8" diameter cylindrical 6" long was measured "as received".

4.2.4 Ag-2.1 at. % Al

This alloy was prepared by Seth and Woods (1970), in the form of a 1 mm diameter wire, and cold-worked by them in the process of drawing through dies, with intermediate anneals.

4.2.5 Gold Alloys

The Au-2 at. % Pt and the Au-10 at. % Ag alloys were prepared by induction melting materials of 99.999 % purity in recrystallized alumina crucibles under argon. Resulting ingots were etched and rolled into square rods of 4 mm² cross-section and 10 cm long.

4.2.6 Palladium

A 50 cm coil of 1 mm diameter pure palladium wire (impurity content <12 ppm) was obtained from a commercial source (Johnson Matthey, 1972) and used as the specimen.

4.3 Annealing

The specimens were annealed in a horizontal vacuum furnace whose temperature could be controlled with an uncertainty of $\pm 5^{\circ}\text{C}$. All annealings were carried out for a period of 12 hours after which the specimen was allowed to cool gradually. The Cu-10 at. & Al specimens were annealed under vacuum but the rest of the specimens were annealed in an atmosphere of argon. To prevent excessive loss of zinc, the brass specimens were placed in a hollow brass cylinder with a loosely fitting cap and annealed under argon.



CHAPTER V

EXPERIMENTAL RESULTS

5.1 Graphical Presentation of Results

The thermal conductivity data for all alloys has been presented in Figs. 4 to 9 as plots of λ/T against T for reasons discussed in Chapter II, and to facilitate comparison with previous work. On these curves, departures from a horizontal straight line through L_0/ρ_0 (denoted by horizontal arrows) represent the contribution of λ_g to the total conductivity where, using eqns. (2.1) and (2.2)

$$\lambda_g = \lambda - (L_0/\rho_0) T \quad (5.1)$$

5.2 Copper Alloys

Data for the Cu-10 at. % Al and Cu-30 at. % Zn alloys, in various states of anneal, have been plotted in Fig. 4 and Fig. 5 respectively. In the temperature region 1.2 to 4 K the thermal conductivity points for the cold-worked and fully annealed states can be fitted to straight lines. However, this is impossible for the partially annealed states. Thus a least squares fit was made in two line segments (Mitchell et al 1971) giving rise to a "kink" in the plots, at a temperature

T_k , around 2.5 to 3 K (indicated by small vertical arrows). Below 1.2 K, thermal conductivity values depart from the T^2 dependence and so the data, in the region 0.5 to 1.2 K, appear as a "bump".

Fig. 6 is a plot of λ/T vs T for the 1/8" diameter Cu-30 at. % Zn single crystal. Square rods cut from the larger crystal yielded basically similar results. The lattice thermal conductivity of this specimen is slightly larger than that of the fully annealed Cu-30 at. % Zn alloy, but the onset temperature of the bump is the same (≈ 1.2 K).

5.3 Silver and Gold Alloys

A plot of Ag-2.1 at. % Al data (Fig. 7) indicates the presence of a "bump" at a slightly lower temperature (≈ 1 K). Between 1 and 4 K the thermal conductivity points cannot be fitted to a straight line so that "kinks" appear at a temperature $T_k \approx 2.5$ K.

Data for the Au-2 at. % Pt and Au-10 at. % Ag alloys are presented in Fig. 8 and Fig. 9 respectively. Kinks are evident in the λ/T vs T plots at $T_k \approx 2$ K, which is lower than the values of T_k for copper and silver alloys. The onset temperature of the bump, T_k , appears to be just below 0.8 K. However, unlike the situation in the silver and copper alloys, the values of

λ_g in the cold-worked condition do not approach the λ_g values of the annealed state at the lowest temperatures.

The residual resistivity of each specimen was measured in various states of anneal and the values are listed in Table 2. The residual resistivity of the Au-2 at. % Pt alloy increased from 1.2 to 2 $\mu\Omega\text{-cm}$ on annealing, and dropped to 1.8 $\mu\Omega\text{-cm}$ on re-rolling. This puzzling phenomenon has been observed previously by Birch et al (1959). Thermal conductivity measurements were made in all three states of anneal.

The measured thermal conductivities and lattice conductivities calculated from them, using eqn. (5.1) with $L_0 = 2.445 \times 10^{-8} \text{ W}\Omega\text{K}^{-2} \pm 1 \%$, are listed as a function of temperature in Tables 3 to 18. Since the measured Lorenz ratio, $\lambda\rho/T$, for the cold-worked gold alloys was less than L_0 at certain temperatures, the calculated λ_g values, at these temperatures, are negative.

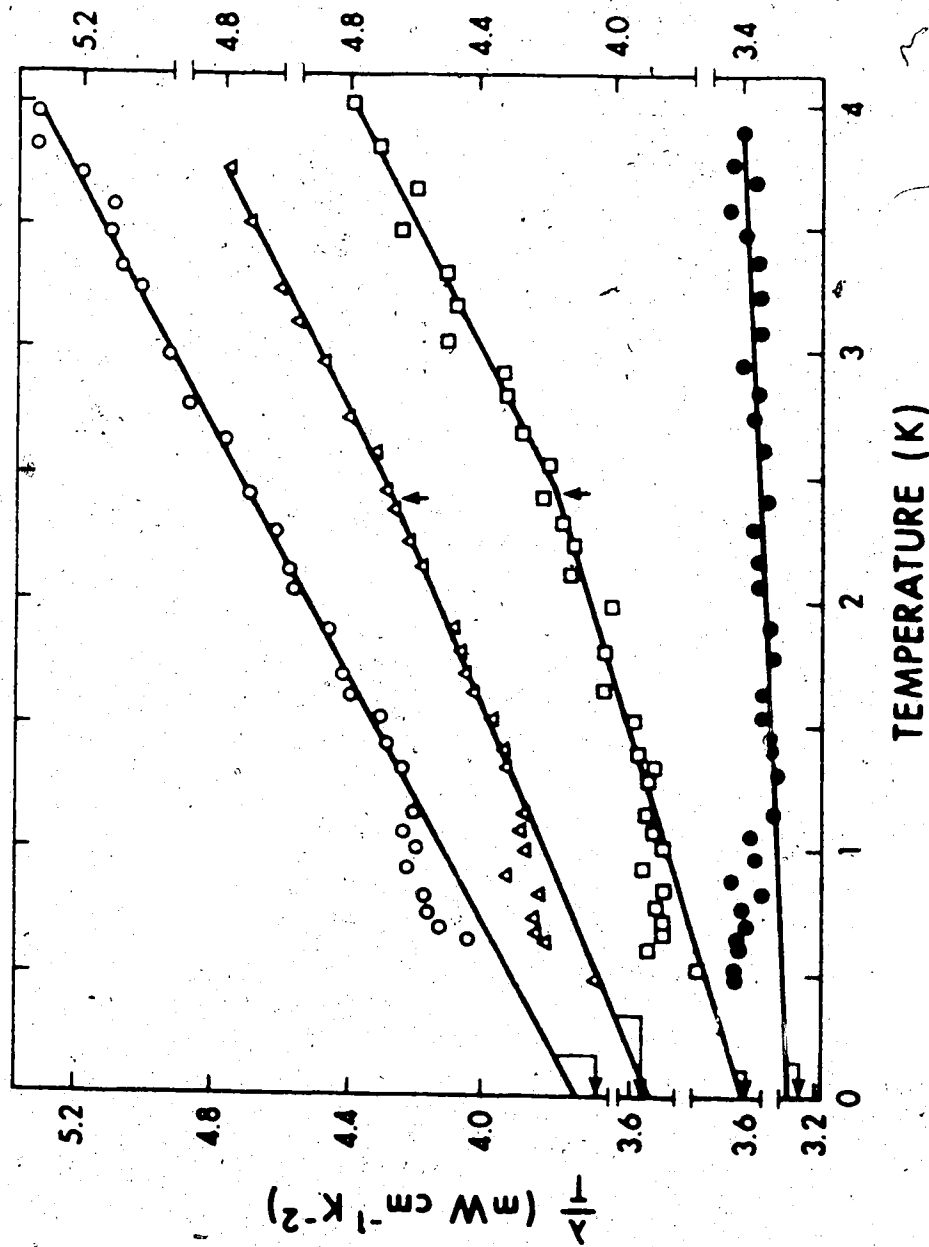


Fig. 4. Ratio of the experimental total thermal conductivity to the absolute temperature is plotted against temperature for the Cu-10% Al alloy. The horizontal arrows indicate the ratio L_0/ρ_0 . The lowest curve represents the specimen in the cold-worked state and each higher curve represents the same specimen in successively higher states of anneal. Annealing temperatures are shown in Table 1.

Table 3

Total thermal conductivity λ and lattice thermal conductivity λ_g in $\text{mW cm}^{-1} \text{K}^{-1}$ as a function of temperature T in degrees K for Cu-10 at. % Al (unannealed).

$$\rho_0 = 7.54 \mu\Omega\text{-cm}$$

$$l/a = 64.2 \text{ cm}^{-1}$$

T	λ	λ_g	T	λ	λ_g
3.894	13.20	0.57±0.13	1.775	5.87	0.12±0.06
3.764	12.88	0.67±0.12	1.634	5.45	0.16±0.05
3.691	12.41	0.44±0.12	1.539	5.26	0.27±0.05
3.584	12.28	0.66±0.12	1.409	4.67	0.10±0.05
3.485	11.80	0.49±0.12	1.304	4.30	0.08±0.04
3.375	11.32	0.38±0.11	1.141	3.78	0.08±0.04
3.236	10.83	0.34±0.11	1.062	3.58	0.14±0.04
3.091	10.35	0.32±0.10	0.968	3.25	0.11±0.03
2.956	10.03	0.45±0.10	0.877	3.00	0.15±0.03
2.843	9.54	0.32±0.09	0.825	2.75	0.08±0.03
2.737	8.72	0.32±0.09	0.771	2.62	0.12±0.03
2.614	8.72	0.25±0.09	0.699	2.36	0.10±0.02
2.409	8.01	0.20±0.08	0.653	2.22	0.10±0.02
2.296	7.72	0.27±0.08	0.609	2.07	0.10±0.02
2.170	7.27	0.23±0.07	0.528	1.80	0.09±0.02
2.064	6.91	0.22±0.07	0.487	1.66	0.08±0.02

Table 4

Total thermal conductivity λ and lattice thermal conductivity λ_g in $\text{mW cm}^{-1} \text{K}^{-1}$ as a function of temperature T in degrees K for Cu-10 at. % Al (annealed 600 K)

$$\rho_0 = 6.79 \mu\Omega\text{-cm}$$

$$l/a = 53.1 \text{ cm}^{-1}$$

T	λ	λ_g	T	λ	λ_g
4.010	19.16	4.71±0.15	1.982	7.94	0.80±0.07
3.836	18.03	4.22±0.14	1.806	7.27	0.77±0.07
3.663	16.79	3.60±0.13	1.645	6.63	0.71±0.06
3.495	16.18	3.59±0.13	1.520	5.99	0.51±0.06
3.323	14.94	2.97±0.12	1.391	5.46	0.47±0.05
3.192	14.26	2.76±0.12	1.279	4.98	0.38±0.04
3.050	13.71	2.73±0.11	1.140	4.45	0.34±0.04
2.922	12.63	2.11±0.11	1.074	4.17	0.30±0.04
2.829	12.22	2.03±0.10	1.010	3.89	0.25±0.03
2.675	11.43	1.80±0.10	0.928	3.63	0.29±0.03
2.558	10.71	1.50±0.09	0.842	3.24	0.21±0.03
2.420	10.18	1.47±0.09	0.712	2.74	0.18±0.02
2.328	9.65	1.28±0.09	0.663	2.56	0.17±0.02
2.231	9.20	1.17±0.08	0.601	2.34	0.18±0.02
2.111	8.71	1.11±0.08	0.515	1.95	0.09±0.02

Table 5

Total thermal conductivity λ and lattice thermal conductivity λ_g in $\text{mW cm}^{-1} \text{K}^{-1}$ as a function of temperature T in degrees K for Cu-10 at.% Al (annealed 675 K).

$$\rho_0 = 6.88 \mu\Omega\text{-cm}$$

$$l/a = 55.7 \text{ cm}^{-1}$$

T	λ	λ_g	T	λ	λ_g
3.744	17.90	4.59±0.14	1.624	6.60	0.83±0.06
3.517	16.60	4.10±0.13	1.521	6.09	0.69±0.06
3.255	15.08	3.51±0.12	1.404	5.58	0.59±0.05
3.119	14.29	3.21±0.11	1.333	5.29	0.55±0.05
2.965	13.35	2.81±0.11	1.146	4.48	0.41±0.04
2.738	12.14	2.41±0.10	1.078	4.23	0.40±0.04
2.603	11.31	2.06±0.09	0.994	3.88	0.35±0.04
2.442	10.55	1.87±0.09	0.903	3.58	0.37±0.03
2.367	10.16	1.74±0.08	0.824	3.19	0.26±0.03
2.235	9.51	1.57±0.08	0.730	2.84	0.24±0.03
2.135	8.99	1.40±0.08	0.668	2.59	0.21±0.02
1.895	7.81	1.07±0.07	0.623	2.40	0.19±0.02
1.796	7.36	0.98±0.07	0.480	1.78	0.08±0.02

Table 6

Total thermal conductivity λ and lattice thermal conductivity λ_g in $\text{mW cm}^{-1} \text{K}^{-1}$ as a function of temperature T in degrees K for Cu-10 at. % Al (annealed 1000 K).

$$\rho_0 = 6.69 \mu\Omega\text{-cm}$$

$$l/a = 59.4 \text{ cm}^{-1}$$

T	λ	λ_g	T	λ	λ_g
3.971	21.18	6.68±0.15	1.883	8.40	1.52±0.07
3.834	20.45	6.44±0.14	1.703	7.52	1.30±0.06
3.723	19.37	5.76±0.14	1.619	7.12	1.20±0.06
3.597	18.36	5.22±0.13	1.533	6.60	1.00±0.06
3.482	17.80	5.08±0.13	1.424	6.11	0.90±0.05
3.347	16.99	4.76±0.13	1.326	5.62	0.77±0.05
3.258	16.35	4.45±0.12	1.144	4.81	0.63±0.04
2.988	14.76	3.84±0.11	1.068	4.52	0.62±0.04
2.791	13.61	3.42±0.10	1.002	4.22	0.55±0.04
2.647	12.62	2.95±0.10	0.925	3.90	0.53±0.03
2.431	11.40	2.54±0.09	0.808	3.37	0.42±0.03
2.278	10.52	2.20±0.09	0.739	3.07	0.37±0.03
2.123	9.72	1.96±0.08	0.686	2.83	0.32±0.03
2.047	9.35	1.87±0.08	0.641	2.59	0.25±0.02

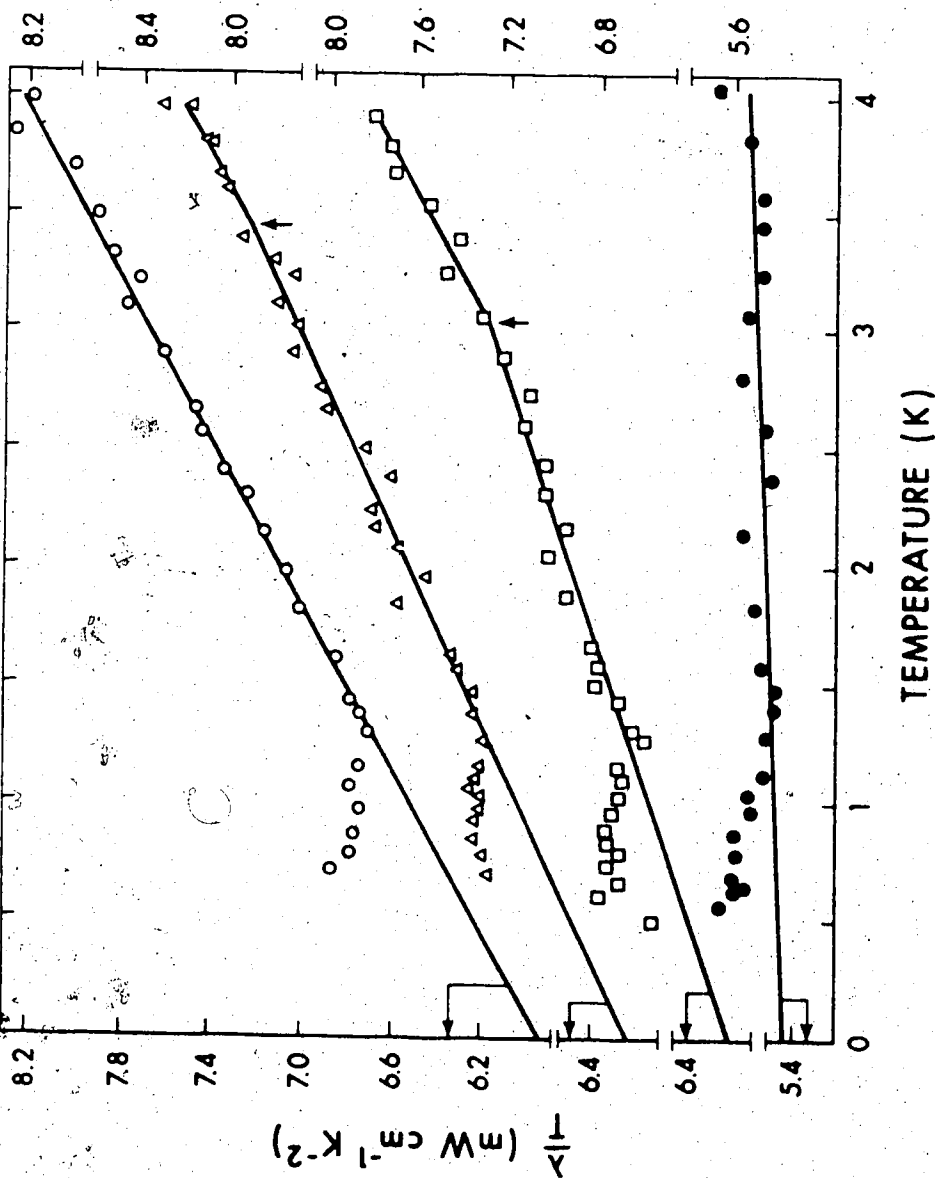


Fig. 5. Ratio of the experimental total thermal conductivity to the absolute temperature is plotted against temperature for the Cu-30% Zn alloy. The horizontal arrows indicate the ratio L_0/ρ_0 . The lowest curve represents the specimen in the cold-worked state and each higher curve represents the same specimen in successively higher states of anneal. Annealing temperatures are shown in Table 1.

Table 7

Total thermal conductivity λ and lattice thermal conductivity λ_g in $\text{mW cm}^{-1} \text{K}^{-1}$ as a function of temperature T in degrees K for Cu-30 at.% Zn (unannealed).

$$\rho_0 = 4.59 \mu\Omega\text{-cm}$$

$$l/a = 61.5 \text{ cm}^{-1}$$

T	λ	λ_g	T	λ	λ_g
4.033	22.85	1.37±0.22	1.480	8.08	0.19±0.08
3.823	21.25	0.88±0.21	1.403	7.67	0.19±0.08
3.582	19.72	0.63±0.20	1.286	7.04	0.19±0.07
3.458	19.05	0.63±0.19	1.124	6.17	0.18±0.06
3.245	17.86	0.57±0.17	1.038	5.76	0.23±0.07
3.080	17.08	0.68±0.17	0.971	5.38	0.21±0.05
2.815	15.69	0.70±0.15	0.872	4.89	0.24±0.05
2.597	14.27	0.44±0.14	0.785	4.40	0.21±0.04
2.371	12.96	0.33±0.13	0.687	3.85	0.19±0.04
2.140	11.92	0.53±0.12	0.635	3.54	0.15±0.04
1.840	10.16	0.36±0.10	0.622	3.48	0.17±0.03
1.581	8.69	0.27±0.09	0.567	3.21	0.19±0.03

Table 8

Total thermal conductivity λ and lattice thermal conductivity λ_g in $\text{mW cm}^{-1} \text{K}^{-1}$ as a function of temperature T in degrees K for Cu-30 at. % Zn (annealed 600 K).

$$\rho_0 = 3.82 \mu\Omega\text{-cm}$$

$$\lambda/a = 67.1 \text{ cm}^{-1}$$

T	λ	λ_g	T	λ	λ_g
3.908	30.50	5.50±0.26	1.580	10.75	0.64±0.10
3.785	29.28	5.07±0.25	1.502	10.22	0.61±0.10
3.673	28.31	4.81±0.24	1.417	9.52	0.46±0.09
3.530	26.70	4.12±0.23	1.306	8.69	0.33±0.09
3.395	25.19	3.47±0.22	1.269	8.38	0.27±0.08
3.241	24.25	3.52±0.21	1.152	7.73	0.36±0.08
3.055	22.34	2.80±0.20	1.098	7.36	0.34±0.07
2.883	20.86	2.41±0.19	1.021	6.86	0.33±0.07
2.730	19.41	1.95±0.18	0.954	6.43	0.33±0.06
2.601	18.56	1.93±0.17	0.889	6.02	0.33±0.06
2.444	17.21	1.57±0.16	0.826	5.58	0.30±0.05
2.313	16.29	1.49±0.15	0.784	5.26	0.25±0.05
2.169	15.06	1.18±0.14	0.730	4.94	0.27±0.05
2.049	14.40	1.29±0.13	0.662	4.44	0.21±0.04
1.880	13.07	1.04±0.12	0.607	4.13	0.24±0.04
1.664	11.38	0.73±0.11	0.497	3.26	0.08±0.03

Table 9

Total thermal conductivity λ and lattice thermal conductivity λ_g in $\text{mW cm}^{-1} \text{K}^{-1}$ as a function of temperature T in degrees K for Cu-30 at. % Zn (annealed 700 K).

$$\rho_0 = 3.78 \mu\Omega\text{-cm}$$

$$l/a = 71.2 \text{ cm}^{-1}$$

T	λ	λ_g	T	λ	λ_g
3.952	32.38	6.78±0.26	2.168	15.94	1.90±0.14
3.810	30.98	6.31±0.25	2.080	15.09	1.61±0.14
3.805	30.79	6.15±0.25	1.960	13.99	1.29±0.13
3.661	29.50	5.79±0.24	1.840	13.36	1.44±0.12
3.600	28.91	5.60±0.24	1.635	11.47	0.88±0.11
3.392	27.02	5.06±0.22	1.567	10.96	0.81±0.10
3.303	25.83	4.44±0.22	1.474	10.21	0.66±0.10
3.231	24.97	4.05±0.21	1.374	9.50	0.60±0.09
3.124	24.34	4.10±0.21	1.263	8.67	0.49±0.08
3.026	23.33	3.73±0.20	1.152	7.93	0.47±0.08
2.907	22.46	3.63±0.19	1.057	7.32	0.47±0.07
2.766	21.03	3.11±0.18	0.971	6.68	0.40±0.06
2.668	20.19	2.91±0.18	0.930	6.42	0.40±0.06
2.510	18.58	2.32±0.17	0.842	5.82	0.36±0.06
2.375	17.30	1.92±0.16	0.775	5.32	0.31±0.05
2.248	16.57	2.01±0.16	0.691	4.72	0.25±0.05

Table 10

Total thermal conductivity λ and lattice thermal conductivity λ_g in $\text{mW cm}^{-1} \text{K}^{-1}$ as a function of temperature T in degrees K for Cu-30 at. % Zn (annealed 1000 K).

$$\rho_0 = 3.86 \mu\Omega\text{-cm}$$

$$l/a = 64.5 \text{ cm}^{-1}$$

T	λ	λ_g	T	λ	λ_g
3.986	32.85	7.61±0.26	2.165	15.83	2.11±0.14
3.826	31.16	6.93±0.25	2.035	14.56	1.67±0.13
3.715	30.04	6.51±0.24	1.829	12.94	1.36±0.12
3.606	28.70	5.86±0.23	1.649	11.38	0.94±0.11
3.473	27.75	5.75±0.22	1.557	10.77	0.90±0.10
3.326	26.24	5.17±0.22	1.416	9.66	0.69±0.09
3.287	25.44	4.62±0.21	1.301	8.80	0.56±0.08
3.216	25.01	4.63±0.21	1.164	7.96	0.58±0.08
3.054	23.77	4.42±0.20	1.090	7.44	0.53±0.07
2.906	22.28	3.87±0.19	1.040	7.10	0.51±0.07
2.803	21.28	3.52±0.18	0.984	6.70	0.47±0.06
2.646	19.85	3.08±0.17	0.910	6.22	0.46±0.06
2.518	18.58	2.63±0.16	0.820	5.56	0.36±0.05
2.346	16.94	2.08±0.15	0.740	5.06	0.36±0.05

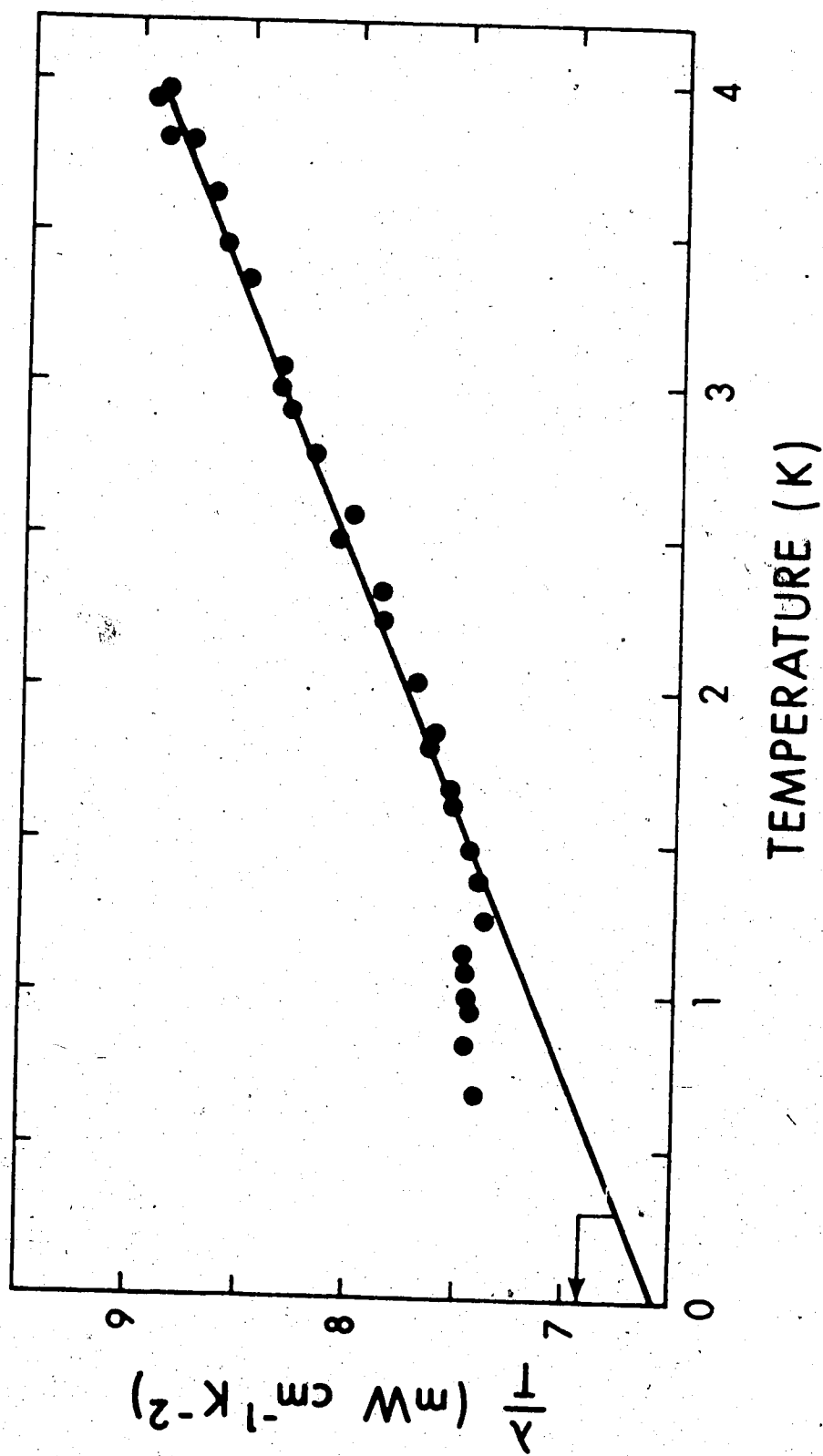


Fig. 6. Ratio of the experimental total thermal conductivity to the absolute temperature is plotted against temperature for the single crystal of brass. The horizontal arrow indicates the ratio L_0/ρ_0 .

Table 11

Total thermal conductivity λ and lattice thermal conductivity λ_g in $\text{mW cm}^{-1} \text{K}^{-1}$ as a function of temperature T in degrees K for Cu-30 at. % Zn Single Crystal.

$$\rho_0 = 3.53 \mu\Omega\text{-cm}$$

$$l/a = 129.7 \text{ cm}^{-1}$$

T	λ	λ_g	T	λ	λ_g
3.991	36.70	8.33±0.29	2.310	18.58	2.16±0.17
3.792	34.26	7.31±0.28	2.156	17.10	1.77±0.16
3.654	32.42	6.45±0.27	2.022	16.22	1.85±0.15
3.475	30.54	5.84±0.26	1.801	14.24	1.43±0.13
3.341	28.89	5.15±0.25	1.606	12.39	0.98±0.12
3.241	27.79	4.76±0.24	1.489	11.41	0.82±0.11
3.197	26.99	4.27±0.24	1.319	9.97	0.59±0.10
2.991	25.36	4.10±0.22	1.250	9.41	0.53±0.09
2.810	23.43	3.46±0.21	1.166	8.86	0.57±0.09
2.774	23.36	3.64±0.20	1.077	8.14	0.48±0.07
2.640	21.56	2.79±0.19	0.971	7.35	0.45±0.07
2.547	20.74	2.63±0.18	0.862	6.52	0.40±0.07
2.430	19.86	2.59±0.17	0.685	5.16	0.29±0.05

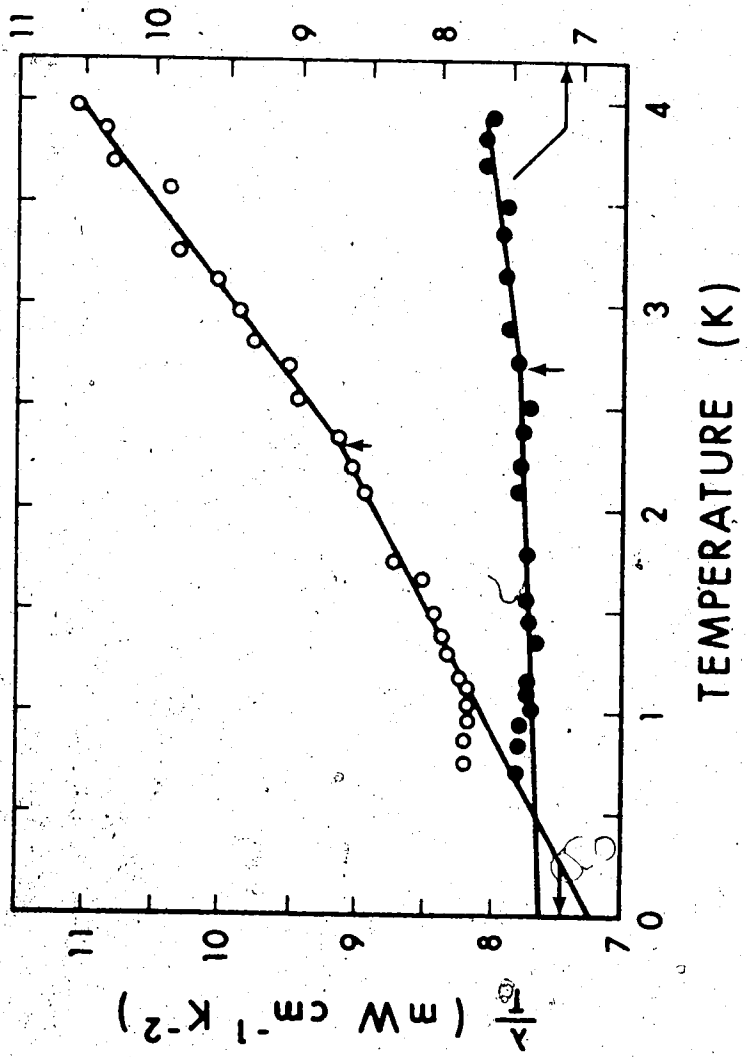


Fig. 7. Ratio of the experimental total thermal conductivity to the absolute temperature is plotted against temperature for the Ag-2.1 & Al alloy. The horizontal arrows indicate the ratio L_0/ρ_0 . The closed circles represent the specimen in the cold-worked state and the scale is given on the right. The open circles represent the specimen in the annealed state. Annealing temperatures are shown in Table 1.

Table 12

Total thermal conductivity λ and lattice thermal conductivity λ_g in $\text{mW cm}^{-1} \text{K}^{-1}$ as a function of temperature T in degrees K for Ag-2.1 at.% Al (unannealed).

$$\rho_0 = 3.43 \mu\Omega\text{-cm}$$

$$l/a = 244 \text{ cm}^{-1}$$

T	λ	λ_g	T	λ	λ_g
3.932	30.04	1.98±0.29	2.085	15.54	0.66±0.16
3.825	29.48	2.19±0.28	1.763	12.99	0.41±0.13
3.688	28.35	2.03±0.27	1.555	11.52	0.42±0.12
3.484	26.24	1.38±0.25	1.444	10.62	0.32±0.11
3.153	23.78	1.29±0.23	1.358	9.89	0.20±0.09
3.352	25.34	1.43±0.25	1.176	8.70	0.30±0.08
2.890	21.73	1.11±0.21	1.099	8.10	0.26±0.08
2.712	20.19	0.84±0.20	1.018	7.47	0.21±0.08
2.498	18.36	0.54±0.18	0.938	6.96	0.27±0.07
2.380	17.65	0.67±0.18	0.834	6.18	0.24±0.07
2.213	16.45	0.67±0.17	0.700	5.23	0.23±0.05

Table 13

Total thermal conductivity λ and lattice thermal conductivity λ_g in $\text{mW cm}^{-1} \text{K}^{-1}$ as a function of temperature T in degrees K for Ag-2.1 at % Al (annealed 1000 K).

$$\rho_0 = 3.27 \mu\Omega\text{-cm}$$

$$l/a = 174.4 \text{ cm}^{-1}$$

T	λ	λ_g	T	λ	λ_g
3.976	44.07	14.36±0.31	2.075	18.55	3.04±0.16
3.843	41.71	12.98±0.30	1.734	15.15	2.18±0.13
3.693	39.87	12.26±0.28	1.648	14.03	1.71±0.13
3.564	36.94	10.30±0.28	1.483	12.49	1.41±0.12
3.249	33.50	9.22±0.25	1.372	11.47	1.22±0.11
3.107	31.12	7.90±0.23	1.290	10.74	1.10±0.10
2.960	29.23	7.10±0.23	1.165	9.59	0.88±0.09
2.829	27.62	6.47±0.22	1.118	9.13	0.77±0.08
2.703	25.70	5.49±0.21	1.032	8.43	0.71±0.08
2.523	23.81	4.95±0.19	0.949	7.74	0.65±0.07
2.352	23.51	3.93±0.17	0.861	7.06	0.62±0.06
2.202	19.93	3.47±0.17	0.759	6.22	0.55±0.06

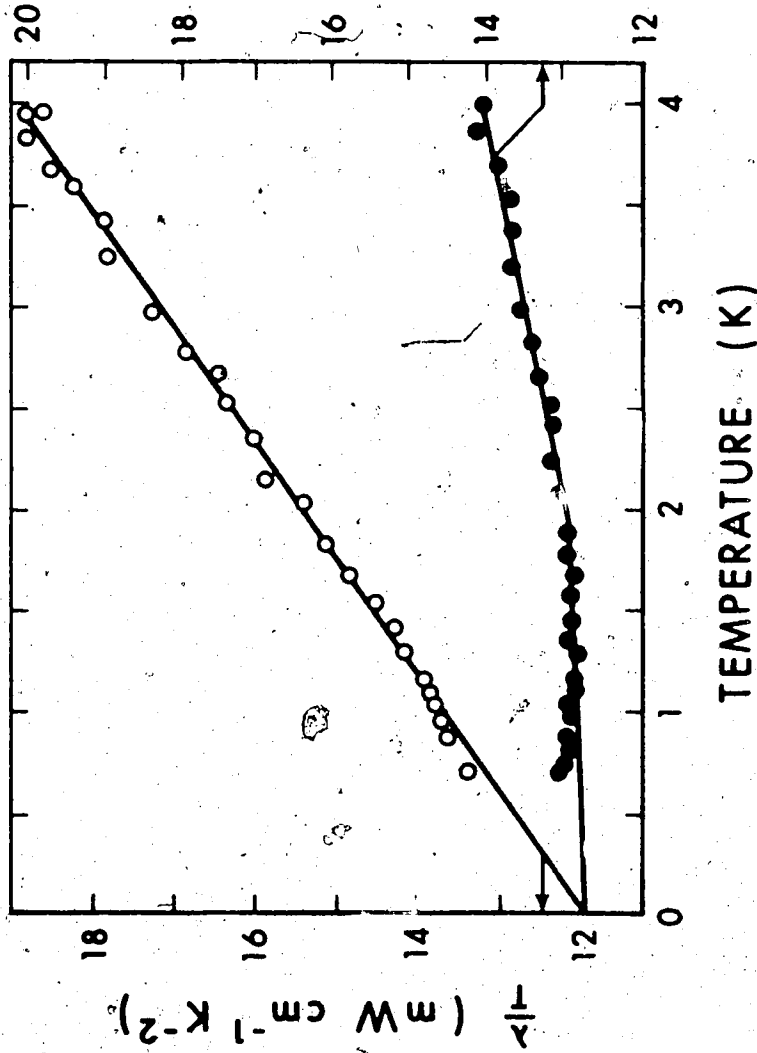


Fig. 8. Ratio of the experimental total thermal conductivity to the absolute temperature is plotted against temperature for the Au-2%Pt alloy. The horizontal arrows indicate the ratio L/ρ_0 . The closed circles represent the specimen in the cold-worked state and the scale is given on the right. The open circles represent the specimen in the annealed state. Annealing temperatures are shown in Table I.

Table 14

Total thermal conductivity λ and lattice thermal conductivity λ_g in $\text{mW cm}^{-1} \text{K}^{-1}$ as a function of temperature T in degrees K for Au-2 at. % Pt (unannealed).

$$\rho_0 = 1.19 \mu\Omega\text{-cm}$$

$$l/a = 214.4 \text{ cm}^{-1}$$

T	λ	λ_g	T	λ	λ_g
3.985	87.14	5.19±0.84	2.053	43.42	1.21±0.43
3.888	84.40	4.45±0.82	1.748	37.05	1.10±0.37
3.772	82.26	4.70±0.79	1.547	32.49	0.67±0.33
3.585	77.58	3.86±0.75	1.370	28.62	0.45±0.29
3.363	72.27	3.11±0.71	1.249	26.01	0.32±0.26
3.047	64.63	1.97±0.64	1.152	24.21	0.52±0.24
2.818	59.53	1.68±0.59	1.070	22.54	0.54±0.23
2.682	56.57	1.42±0.56	0.967	20.37	0.49±0.20
2.500	51.47	1.46±0.52	0.891	18.81	0.49±0.18
2.315	49.06	1.46±0.49	0.778	16.41	0.41±0.16
2.139	45.42	1.44±0.45	0.681	14.52	0.51±0.14

Table 15

Total thermal conductivity λ and lattice thermal conductivity, λ_g in $\text{mW cm}^{-1} \text{K}^{-1}$ as a function of temperature T in degrees K for Au-2 at. % Pt (annealed and then rolled).

$$\rho_0 = 1.84 \text{ } \mu\Omega\text{-cm}$$

$$l/a = 206.2 \text{ cm}^{-1}$$

T	λ	λ_g^*	T	λ	λ_g^*
3.985	55.90	3.01±0.54	1.777	23.07	-0.52±0.24
3.868	54.60	3.25±0.52	1.669	21.47	-0.68±0.23
3.696	51.21	2.15±0.50	1.573	20.31	-0.57±0.21
3.526	48.28	1.47±0.48	1.458	18.81	-0.54±0.20
3.372	46.11	1.35±0.46	1.355	17.57	-0.41±0.18
3.183	43.56	1.31±0.43	1.283	16.44	-0.59±0.17
2.987	40.54	0.89±0.41	1.160	14.91	-0.48±0.16
2.822	37.81	0.35±0.38	1.105	14.16	-0.50±0.15
2.634	35.18	0.10±0.36	1.046	13.53	-0.36±0.14
2.511	33.10	-0.23±0.34	0.976	12.59	-0.37±0.13
2.406	31.61	-0.33±0.33	0.885	11.48	-0.26±0.12
2.238	29.49	-0.22±0.30	0.810	10.47	-0.28±0.11
2.074	27.12	-0.41±0.28	0.733	9.53	-0.20±0.10
1.880	24.34	-0.61±0.26	0.706	9.24	-0.13±0.10

* Negative values for λ_g explained in section 6.3.

Table 16

Total thermal conductivity λ and lattice thermal conductivity λ_g in $\text{mW cm}^{-1} \text{K}^{-1}$ as a function of temperature T in degrees K for Au-2 at. \% Pt (annealed 1000 K).

$$\rho_0 = 1.97 \mu\Omega\text{-cm}$$

$$l/a = 279.6 \text{ cm}^{-1}$$

T	λ	λ_g	T	λ	λ_g
3.960	73.42	24.14±0.50	2.025	31.12	5.93±0.26
3.836	72.00	24.27±0.49	1.825	27.58	4.88±0.23
3.668	67.80	22.16±0.47	1.667	24.67	3.93±0.21
3.587	65.26	20.63±0.46	1.537	22.28	3.16±0.20
3.421	60.99	18.42±0.43	1.415	20.16	2.56±0.18
3.248	57.01	16.60±0.41	1.298	18.35	2.20±0.17
2.964	51.07	14.19±0.38	1.148	15.99	1.71±0.15
2.776	46.76	12.22±0.35	1.094	15.16	1.55±0.14
2.669	43.91	10.70±0.34	1.025	14.11	1.36±0.13
2.517	41.13	9.81±0.32	0.948	12.97	1.18±0.12
2.345	37.57	8.40±0.30	0.862	11.76	1.03±0.11
2.140	33.95	7.32±0.27	0.703	9.42	0.67±0.09

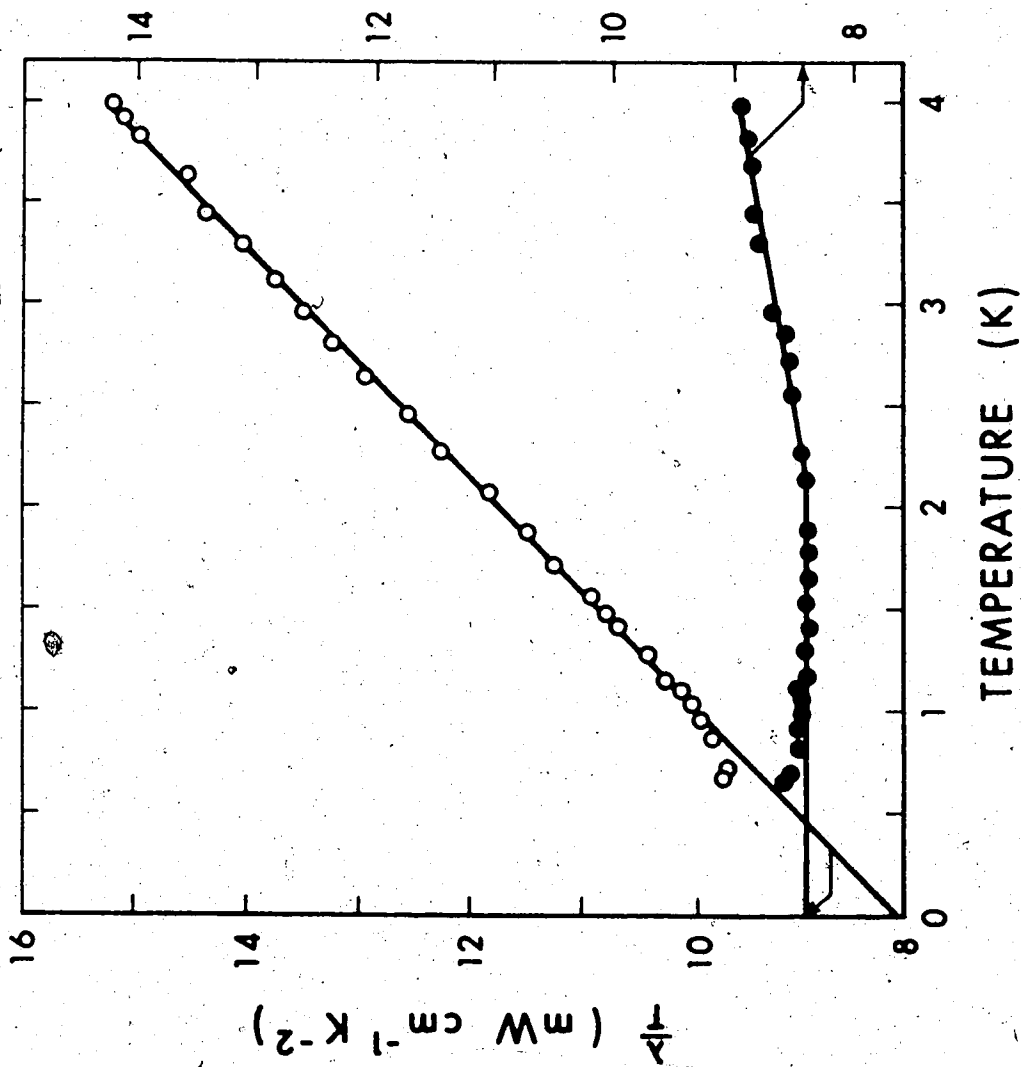


Fig. 9. Ratio of the experimental total thermal conductivity to the absolute temperature is plotted against temperature for the Au-10% Ag alloy. The horizontal arrows indicate the transition from the cold-worked state to the annealed state. The open circles represent the specimen in the cold-worked state and the closed circles represent the specimen in the annealed state. Annealing temperatures are shown in Table 1.

Table 17

Total thermal conductivity λ and lattice thermal conductivity λ_g in $\text{mW cm}^{-1} \text{K}^{-1}$ as a function of temperature T in degrees K for Au-10 at. % Ag (unannealed).

$$\rho_0 = 2.90 \mu\Omega\text{-cm}$$

$$l/a = 195.3 \text{ cm}^{-1}$$

T	λ	λ_g^*	T	λ	λ_g^*
3.975	35.60	2.05±0.34	1.644	13.79	-0.09±0.14
3.816	33.93	1.71±0.33	1.523	12.83	-0.03±0.13
3.686	32.74	1.62±0.32	1.409	11.82	-0.07±0.12
3.439	30.42	1.39±0.30	1.295	10.92	-0.02±0.11
3.288	28.96	1.20±0.28	1.160	9.76	-0.03±0.10
2.961	25.76	0.76±0.26	1.116	9.48	0.06±0.10
2.852	24.44	0.36±0.25	1.059	8.96	0.02±0.09
2.709	23.14	0.27±0.23	0.989	8.36	0.01±0.09
2.552	21.81	0.26±0.22	0.913	7.75	0.04±0.08
2.271	19.21	0.04±0.20	0.813	6.89	0.03±0.07
2.134	17.96	-0.06±0.18	0.692	5.92	0.09±0.06
1.883	15.85	-0.05±0.16	0.658	5.65	0.10±0.06

* Negative values for λ_g explained in section 6.3.

Table 18

Total thermal conductivity λ and lattice thermal conductivity λ_g in $\text{mW cm}^{-1} \text{K}^{-1}$ as a function of temperature T in degrees K for Au-10 at. % Ag (annealed 1000 K).

$$\rho_0 = 2.71 \mu\Omega\text{-cm}$$

$$l/a = 148.3 \text{ cm}^{-1}$$

T	λ	λ_g	T	λ	λ_g
3.971	60.32	24.45±0.37	1.872	21.50	4.59±0.18
3.817	57.10	22.61±0.35	1.710	19.24	3.79±0.16
3.628	52.78	20.00±0.33	1.558	17.02	2.94±0.14
3.438	49.45	18.38±0.31	1.405	14.98	2.28±0.13
3.283	46.07	16.40±0.30	1.263	12.93	1.52±0.12
3.113	42.82	14.69±0.29	1.155	11.84	1.40±0.10
2.952	39.86	13.19±0.28	1.113	11.26	1.20±0.10
2.800	37.07	11.78±0.26	1.036	10.39	1.03±0.10
2.634	34.13	10.34±0.25	0.960	9.55	0.88±0.09
2.457	30.85	8.65±0.22	0.855	8.43	0.71±0.08
2.263	27.77	7.33±0.21	0.717	6.97	0.49±0.07
2.070	24.48	5.78±0.20	0.670	6.52	0.46±0.06

CHAPTER VI

DISCUSSION OF MODELS AND EXPERIMENTAL RESULTS

The thermal conductivity results of copper alloys will first be discussed. In section 6.1 it is shown that the anomalies lie in W_{gd} (phonon scattering by dislocations) and in section 6.2 the copper alloy data is discussed with reference to various existing models. Results for the silver and gold alloys are discussed in section 6.3 and finally, in section 6.4, the temperatures at which the anomalies occur are correlated with phonon wavelengths.

6.1 Copper Alloys

From the Cu-10 at. % Al and Cu-30 at. % Zn alloy results shown in Fig. 4 and Fig. 5 respectively, we observe:-

- (i) A change in the temperature dependence of λ around 2.5 to 3 K, referred to as the "kink".
- (ii) An excess conductivity appears below 1.2 K referred to as a "bump".
- (iii) Annealing successively at higher temperatures increases the lattice conductivity but the fractional increases in λ_g at the lowest temperatures are much smaller than at 4 K.

It will first be shown that all these anomalies lie in the lattice component λ_g . They cannot arise from the electronic component λ_e , as any changes in λ_e would be reflected as changes in the electrical resistivity of the specimen through the Weidemann-Franz Law, eqn. (2.2). The electrical resistivity of both the Cu-Al and Cu-Zn alloys was measured, and found to be constant to within 1/2%, over the temperature range 0.5 to 4 K. Therefore, unless a conduction process in addition to phonons and electrons is present, the anomalies must be in λ_g .

6.1.1 Scattering of phonons by electrons or defects?

Having shown that the anomalies are in λ_g the question arises whether they are in W_{gd} (phonon scattering by defects) or W_{ge} (phonon scattering by electrons)? The author believes the kink to be a change in phonon scattering by defects. In Fig. 4 the annealed alloy has the largest λ_g , implying smallest W_{gd} . However, the kink is absent. The kink is present in partially annealed alloys and is more pronounced in the specimen with greater cold-work i.e. larger W_{gd} . The most cold-worked specimen is apparently an exception since it has no kink. In this case, however, the slope is so small that the presence or absence of a kink is unobservable. The author, therefore, disagrees with

Mitchell et al (1971) who ascribed the kink to W_{ge} . Although other large scale defects, which anneal out of cold-worked specimens, could account for these results and the results of other authors above 1.5 K, dislocations seem likely to dominate the phonon scattering in cold-worked specimens (Klemens 1958).

Below 1.2 K the thermal conductivity points lie above the line extrapolated from high temperature measurements (Fig. 4 and Fig. 5). This excess conductivity is also believed to be a feature of W_{gd} and not W_{ge} . Since λ_g in the cold-worked state is very much smaller than in the annealed state, $W_{gd} \gg W_{ge}$ in the cold-worked state. The excess conductivity persists in the cold-worked state indicating that the bump is a component of W_{gd} and is interpreted as a non-standard decrease in W_{gd} below 1.2 K. The interpretation is not so straightforward in the annealed alloys since the relative size of W_{ge} and W_{gd} is unknown and the former could also be anomalous. The simplest explanation is that the anomalies are in W_{gd} in all states of anneal. This makes it necessary to assume that even in the fully annealed state, W_{gd} is still of measurable size and has a similar temperature dependence as for the cold-worked state. Below 0.7 K, λ/T curves are a much less rapid function of cold-work than above 1.5 K. This suggests that below 0.7 K, W_g for the fully annealed

alloys should be a good estimate for W_{ge} . Previous estimates of W_{ge} , based on data above 1.5 K, would thus be too large.

2.2 Estimates of electron limited lattice conductivity

In section 2.2.1 it was shown that the electron limited lattice thermal conductivity, λ_e , is proportional to T^2 at low temperatures. Klemens (1958) has calculated $W_{ge} T^2$ for pure copper and shown that it would be fairly constant on alloying. In Fig. 10, the observed values of $W_g T^2$ for Cu-Zn alloys, pure copper, and a single Cu-Fe alloy, obtained from a number of sources, are shown plotted against impurity concentration. It is evident from this figure that $W_g T^2$ obtained from Kemp et al (1957) increases with concentration and the reasons for this are controversial. White and Woods (1954) evaluated $W_g T^2$ for a Cu-0.056 at. % Fe specimen and obtained a value in close agreement with the theoretical value of $W_{ge} T^2$ (Klemens 1958). The values of $W_g T^2$ obtained from the annealed Cu-Zn alloy and single crystal reported here, (in the region 1-4 K) are approximately the same as those of Kemp et al (1957), for similar concentrations. However, values of $W_g T^2$, evaluated by extrapolating the few measurements below 0.7 K through $L_0 \pm 1\%$, give an estimate of

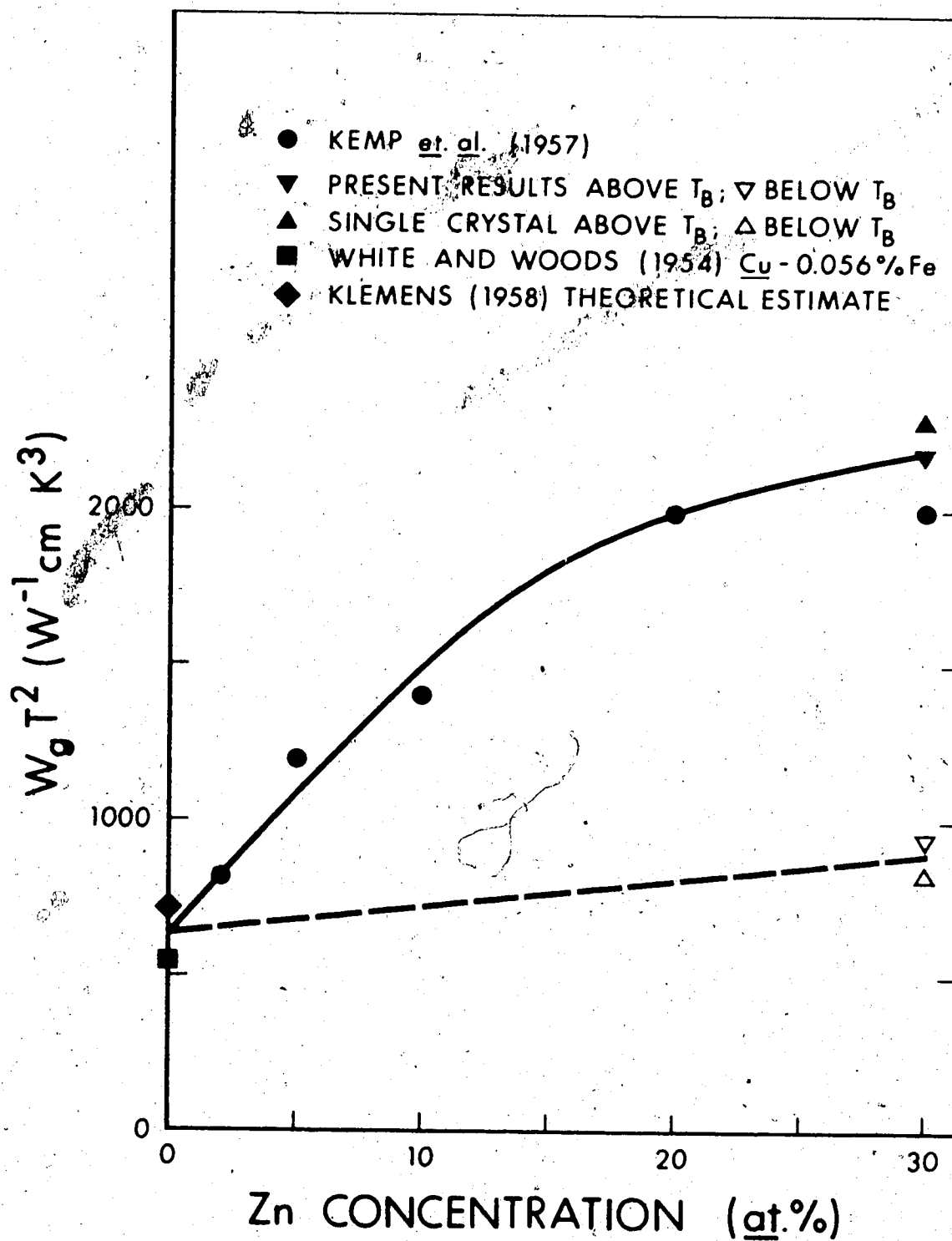


Fig. 10. $W_g T^2$ is plotted against concentration for Cu-Zn alloys.

W_{ge} are much closer to the value in pure copper, as might be expected from the arguments presented above.

6.1.3 Brass, single crystal

Having shown that the anomalies probably arise due to changes in phonon-dislocation scattering, a brass (Cu-30 at. % Zn) single crystal with a low concentration of dislocations (see section 7.2) was measured. Fig. 6 shows that the bump persists and is similar to that in the annealed polycrystalline specimen (Fig. 5). This result is in agreement with measurements of Salter and Charsley (1967) above 1.5 K, on a Cu-12 at. % Al single crystal which has had a lattice conductivity similar to an annealed polycrystalline sample of the same concentration.

6.2 Existing Models

As pointed out in Chapter II, various models have been proposed to explain the anomalous behaviour in λ_g of copper alloys (of comparable ρ_0) around 2-3 K, and predictions have been made of enhanced conductivities in the ^3He region. Two categories of models, already described in Chapter II, involve phonon scattering by either (a) static dislocations or (b) mobile dislocations. We will first discuss our data in terms of the static

dislocation model.

6.2.1 Static dislocations

(a) Dipole model

Leaver and Charsley (1971) have calculated the temperature dependence of λ_g using the dislocation dipole model. They had evidence from electron microscope data, that in their Cu-Al and Cu-Zn specimens, only 20% of the dislocations were in dipole configuration and the dislocation separation, d , for these dipoles was $\approx 200 \text{ \AA}$. Following their method of analysis, detailed computer calculations were made by varying a parameter n and choosing different values for d (100 to 300 \AA).

Over the temperature range 1.2 to 4 K, there is fairly good agreement between the calculated curves and our experimental data. However, below 1.2 K, the calculated λ_g values lie much below the experimental values. It was found that slightly better agreement was obtained below 1.2 K, if a greater fraction of dislocations were assumed to be in dipole formation. However, although the λ_g/T vs T plots appear to be of the right form, and some modification may fit the data exactly, the Leaver and Charsley model, with realistic parameters, cannot explain the enhanced conductivities.

(b) Dislocation rearrangement model

On the basis of their dislocation rearrangement model, Ackerman and Klemens (1971) have shown that the onset temperature, T_B , of excess conductivities in the ^3He region depends on (a) the ratio of the lattice conductivity in the annealed state to that in the deformed state and (b) the density of dislocations in the deformed state N_d . Calculations using $N_d \approx 10^{11} \text{ cm}^{-2}$ and $\lambda_g(\text{annealed})/\lambda_g(\text{deformed}) \approx 3$ yield $T_B \approx 1.2 \text{ K}$. On annealing, N_d decreases and T_B should also decrease. It is evident from the results on Cu-Al and Cu-Zn (Fig. 4 and Fig. 5) that T_B is independent of dislocation densities in contradiction to the predictions of Ackerman and Klemens (1971).

6.2.2 Mobile dislocations

Both the models discussed above lead to a reduction in phonon-dislocation scattering, and thereby an increase in the lattice conductivity, when the phonon wavelengths become larger than some critical value.

Two other models, (based on vibrating dislocations) have also been proposed -- (a) scattering of phonons by mobile dislocations (Ziman 1960) and (b) resonant scattering of phonons by vibrating partial dislocations.

(a) Ziman (1960) has shown that the scattering of phonons by mobile dislocations leads to $W_{gd} \propto T^{-4}$ i.e. $\lambda_g \propto T^4$, at low temperatures. For all the data plotted, at no point in the temperature range 0.5 to 4 K does the lattice conductivity have this strong a temperature dependence.

(b) More recently, Kronmüller (1972) has calculated the vibrational frequencies of partial dislocations in cold-worked, face-centred cubic metals. These frequencies correspond to dominant phonon frequencies around 1 K so that resonant scattering may occur. Resonant scattering of phonons is observed as a change in the temperature dependence of the lattice conductivity, at a temperature corresponding to the resonant frequency ω_0 . Kronmüller has also shown that there should be two such frequencies, one for partial edge dislocations and another, at approximately twice the frequency for partial screw dislocations. In a given alloy, ω_0 is related to the stacking fault energy γ by eqn. (2.7) so that copper alloys with different stacking fault energies should show resonant scattering at different temperatures. Values of stacking fault energies obtained from Saada (1966) show that $\gamma(\text{Cu-30 at. \% Zn})/\gamma(\text{Cu-10 at. \% Al}) \approx 2$ so that $T_B(\text{Cu-30 at. \% Zn})/T_B(\text{Cu-10 at. \% Al})$ and $T_K(\text{Cu-30 at. \% Zn})/T_K(\text{Cu-10 at. \% Al})$ should be. However, from the results on Cu-Al and Cu-

(Fig. 4 and Fig. 5) it is evident that T_B is 1.2 K and $T_k \sim 3$ K for both alloys, which is evidence that Kronmüller's mechanism is not responsible. Further evidence is supplied by comparing the thermal conductivity of a cold-worked Cu-2 at. % Al alloy (Salter and Charsley 1967) with the results on Cu-10 at. % Al reported here. Although the two alloys have widely different stacking fault energies (Saada 1966), the temperature of the kink (≈ 3 K) is the same for both specimens.

Anomalies in λ_g , of the same order of magnitude as the bumps reported here, have been observed in potassium chloride (Pohl 1962), superconducting niobium (Anderson et al 1973) and in some copper alloys (Linz et al 1974), and have been associated with the resonant scattering of phonons. Linz et al (1974) are the only group who have reported a definite minimum in λ_g . Determining the presence or absence of minima in λ_g is important as only Kronmüller's model can explain a minimum in λ_g at around 1 K. The shape of λ_g against T plots is strongly dependent on the accuracy of the experimental Lorenz number, L . In our heavily cold-worked specimens, a shift of L_0 by $\pm 1\%$ can either introduce or eliminate a minimum in λ_g . For all other states of anneal, where, because λ_g is a larger proportion of λ , the accuracy of L is not so critical, no minimum is observed.

Thermal conductivity results of Linz et al (1974) are different, on this point, in that they observe a minimum in the lattice conductivity of copper alloys, in all states of anneal, around 1 K. It is the author's opinion that it is outside the range of the state-of-the-art to be certain that minima do exist in the cold-worked alloys. However, our results for the partially and fully annealed alloys are accurate enough to eliminate the possibility that minima exist. Further work is probably necessary to resolve the difference.

6.2.3 Summary

Following the discussion on static dislocation models in section 6.2.1, it can be concluded that neither the dislocation-dipole model (Leaver and Charsley 1971) nor the dislocation-rearrangement model (Ackerman and Klemens 1971) can adequately explain our results. Of the two mobile dislocation models, it has been shown that the one proposed by Ziman (1960) is not applicable to the results reported here. The other model (Kronmüller 1972) is the only one that can explain the presence of a minimum in the lattice conductivity, though stacking fault energy considerations show even this model to be inconsistent with our data. It is concluded therefore that none of the models discussed so far can adequately

explain our results. However the anomalies were determined to be in λ_g and associated with changes in dislocation scattering. Although the Leaver and Charsley (1971) model does not fit our data, it is believed that some modification of their model can produce a much better fit. The main feature is the assumption of a "characteristic" length, of the order of a few hundred angstroms, associated with the dislocation structure.

6.3 Silver and Gold Alloys

From the arguments in section 6.2 it was concluded that the λ_g anomalies in copper alloys were due to changes in the phonon-dislocation scattering, involving a characteristic length. This conclusion was tested by measurements on other noble metal hosts, where, due to changes in the Debye temperature, phonon wavelengths and dislocation vibrational frequencies would be different and so the anomalies in λ_g would occur at different temperatures.

For each silver and gold alloy specimen, measurements were made only in highly cold-worked and fully annealed states. The temperature of the kink, T_k , for the Ag-2.1 at. % Al (Fig. 7) is roughly -2.5 K and T_B , the onset temperature of the excess conductivity is 1 K.

The presence of a slight kink around 2.5 K for the fully annealed specimen is probably due to the annealing temperature not being sufficiently high. For the gold alloys (Fig. 8 and Fig. 9), T_k is ~2 K and measurements do not extend to a low enough temperature to show a complete bump, since T_B is below 0.8 K. The arguments which have been used to determine the cause of the kink and the excess conductivity bump in copper alloys also apply to the silver and gold alloys. Thus we concluded that the anomalies in all the alloys occur in W_{gd} (scattering of phonons by dislocations).

For the cold-worked gold alloys the measured Lorenz number, at certain temperatures, had a value less than the classical value of $2.445 \times 10^{-8} \text{ W}\Omega\text{K}^{-2}$. Consequently when λ_g was calculated, using eqn. (5.1), negative values for λ_g were obtained, at those temperatures. This can be regarded as an extreme case of a minimum and can be explained, as before, as a cumulative error affecting the lattice conductivity. The Au-2 at. % Pt alloy was measured first in the cold-worked state and the calculated λ_g values (using eqn. (5.1)) were all positive. After annealing and re-rolling it was found that the residual resistivity had increased by a factor of two and λ_g values decreased proportionately. The lattice conductivity values at some temperatures were now negative but the shape of

λ/T against T plots was the same so that both T_k and T_B were unaffected. It is possible that a mistake was made in measuring ρ_0 in the re-rolled state.

6.4 "Effective" Phonon Wavelengths

The apparent similarity of λ_g for alloys with the same host and the difference between alloys with different hosts can be explained by considering the phonon wavelengths in the hosts. Carruthers (1961) defines an "effective wavelength $\bar{\lambda}$ " characterizing those phonons most important in conduction at low temperatures by

$$\bar{\lambda} = 0.6 d (0/T) \quad (6.1)$$

where d is the lattice constant and 0 the Debye temperature of the lattice. Values for these quantities are listed in Table 19. It may be observed that the effective wavelength is nearly the same in copper, silver and gold at T_B , the temperature immediately below which the excess conductivity appears. The temperature of the kink, T_k , changes in a similar manner to T_B but since T_k is less well defined than T_B a quantitative estimate has not been made. The systematic change in T_B and T_k is further evidence that the lattice conductivity is involved and that the conductivity is limited by scattering centres, characterized by the same separation in each metal investigated.

Table 19

Effective wavelengths at T_B

Metal	θ^a (K)	$d^{b,c}$ (Å)	T_B (K)	$\bar{\lambda} = \frac{0.6d\theta}{T_B}$ (Å)
Copper	344	3.6	1.2	620
Silver	225	4.1	1.0	555
Gold	165	4.1	0.75	540

^aObtained from Corak et al (1955).

^bObtained from Pearson (1958).

CHAPTER VII

SUGGESTIONS FOR FURTHER WORK

There are three areas in which preliminary investigations have produced interesting results:

- (a) Superconductors
- (b) Electron Microscopy
- (c) Amorphous Materials.

Since the work described here is preliminary, the suggestions made in this chapter are of a speculative nature compared to the rest of the thesis. It is hoped that the following discussion will give direction to further research in the study of phonon-defect scattering.

7.1 Superconductors

In a superconducting alloy, as the temperature is reduced below the critical temperature T_c , some of the electrons condense into the superconducting ground state. These electrons neither carry heat nor scatter phonons resulting in: (a) a decrease in the electronic conductivity, λ_e and (b) a decrease in W_{ge} thereby increasing the lattice conductivity, λ_g . Consequently, at a temperature $T \lesssim 0.2 T_c$, it may be assumed that the

total measured thermal conductivity is due to phonon conduction limited by scattering from defects.

Measurements made by Anderson and Smith (1973) on single crystal niobium samples exhibited anomalous lattice conductivities between 0.1 and 2 K. They attributed their results to the resonant scattering of phonons by mobile dislocations because the mean free path of phonons passed through a minimum at a temperature near 0.5 K.

One could choose various superconducting materials, with different stacking fault energies and Debye temperatures, and put them to the same series of tests as the noble metal alloys. It would then be interesting to see if correlations existed between the temperatures of the anomalies and values of Debye temperatures or stacking fault energies of the alloys.

7.2 Electron Microscopy

Following the arguments in section 6.1, it seems that all the anomalies in our results could be explained on the basis of phonon scattering by dislocations and their associated strain fields. Table 19 indicates that the "characteristic" length associated with the dislocation structure, in all the alloys, should be of the order of a few hundred angstroms. Consequently, a preliminary investigation of the dislocation structure in



Figure 11. Electron micrographs of annealed Cu-Al (upper) and brass single crystal (lower) showing preferential etching. Scale 1 mm is 100 Å.

the specimens reported here, was made with the electron microscope.

In collaboration with the Physics Department electron microscopy group, specimens of the annealed copper alloys were prepared and studied under the microscope. This investigation was limited to a single sample of each specimen and failed to show any dislocation structure necessary to explain our results. In the brass single crystal the dislocation density was $\sim 10^8 \text{ cm}^{-2}$ and the annealed Cu-10 at. % Al alloy had a dislocation density of the same magnitude. The annealed Cu-30 at. % Zn alloy showed an extremely high density of dislocation. This was probably not characteristic of the bulk specimen but due to the considerable problems involved in preparing a specimen for electron microscopy. However, other interesting features were observed in both the Cu-10 at. % Al and the brass single crystal and these are shown in Fig. 11. These electron micrographs show surface variations of the sample thickness, which is indicative of preferential etching, in regions of $\sim 100\text{-}500 \text{ \AA}$. This suggests the presence of a microstructure of a few hundred \AA which could lead to anomalous scattering for phonons of $\sim 100\text{-}500 \text{ \AA}$ wavelength.

7.3 Amorphous Materials

Zeller and Pohl (1971) measured the thermal

conductivity of some amorphous materials in the temperature range 0.05 to 100 K and their results, for Pyrex and selenium, along with our data on Cu-10 at. % Al, are presented in Fig. 12. The lattice conductivity of both the amorphous materials and the copper alloy is of the same order of magnitude and all the curves have the same characteristic shape with a plateau, though those for the copper alloy are much narrower and at a lower temperature. Morgan and Smith (1974) proposed a very general model of phonon scattering by structural disorder to explain the experimental results on amorphous materials. Their model contains two correlation lengths associated with some order in the solid. Their calculations show that λ_g decreases approximately as T^2 in two regions separated by a plateau as shown in Fig. 12. With correlation lengths of 10 \AA and 1000 \AA they obtained results similar to those for the amorphous materials but longer range correlations would shift the plateau to lower temperatures. It is possible that the similarity of results for noble metals and amorphous materials may not be entirely fortuitous. Hopefully, there will emerge a very general model to explain the behaviour of lattice conductivity in a variety of materials, at low temperatures.

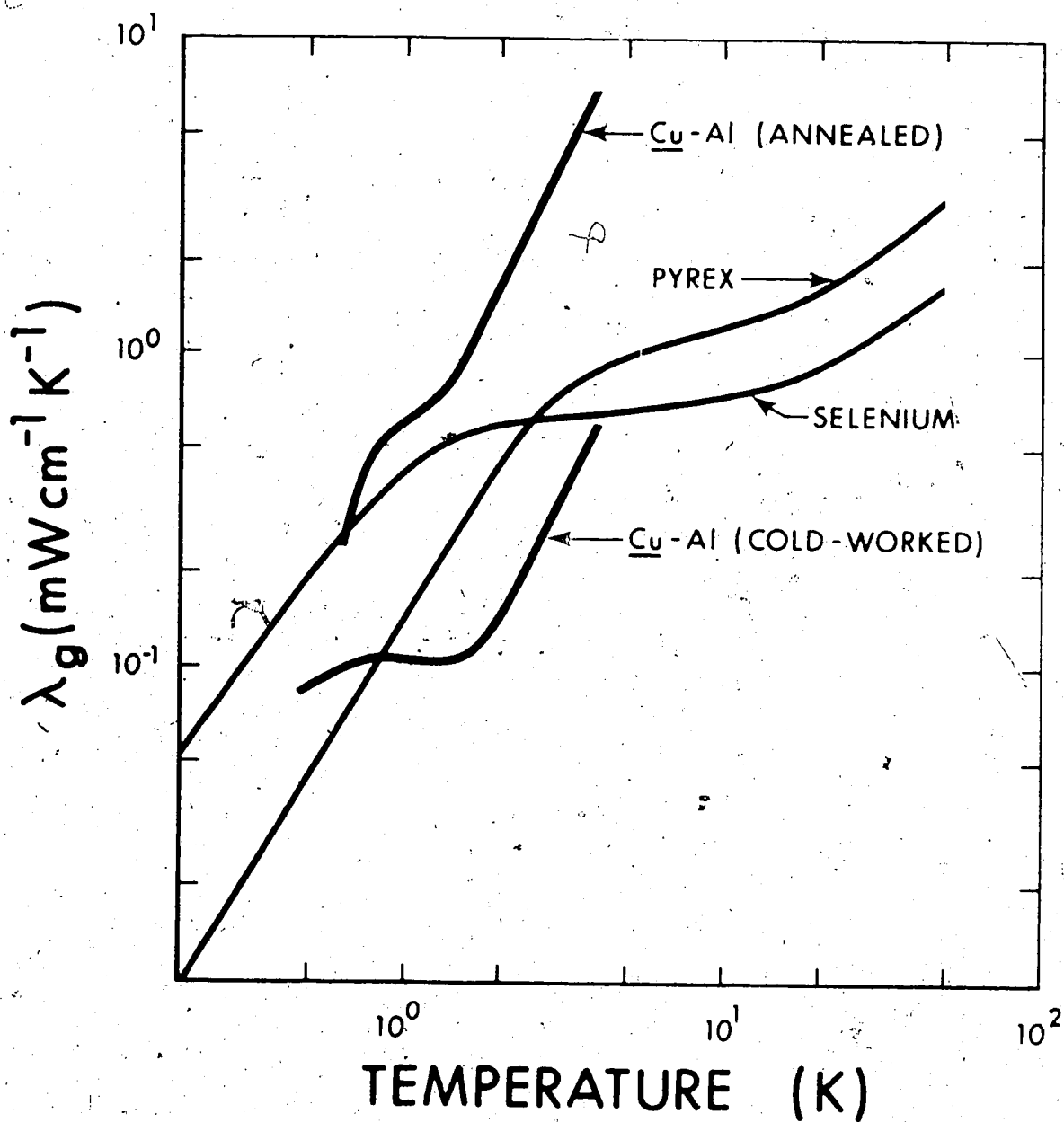


Fig. 12. Lattice thermal conductivity is plotted against temperature for some amorphous materials and Cu-Al alloys.

CHAPTER VIII

CONCLUSIONS

Measurements of the thermal conductivity λ of deformed alloys of copper, silver and gold confirmed the presence of a non-linearity or kink in λ/T vs T plots near 3 K. In the copper and gold alloys, this kink disappeared when the specimens were sufficiently annealed. There was no evidence of any temperature variation of the electrical resistivity in these alloys below 4 K. It is therefore concluded that the kink arose in the lattice conductivity and that it must have been the result of scattering processes that were diminished by annealing.

An excess thermal conductivity, above that expected, occurred in each of these alloys below a temperature T_B near 1 K. Although annealing did not remove this excess conductivity it was also ascribed to a decrease of the phonon scattering by defects below T_B . Both the temperature of the kink and bump varied with the host metal of the alloy which suggests that the anomalies in λ_g are associated with phonons of the same wavelength in all noble metal hosts.

Preliminary electron microscope measurements on copper alloys do not indicate the presence of a dislocation structure with an associated "characteristic"

length. However, there is some evidence of other structures of a few hundred angstroms in size, which could be the scattering centres involved. It is the author's opinion that for further progress thermal conductivity measurements need to be made in conjunction with electron microscopy. There is empirical evidence, supported by Morgan and Smith's model, that similar mechanisms are responsible for the behaviour of λ_g in a variety of materials at low temperatures.

BIBLIOGRAPHY

- Abel W.R., Anderson W.C. and Wheatley J.C. (1964),
Rev. Sci. Instr. 35, 444.
- Ackerman M.W. and Klemens P.G. (1971), Phys. Rev. B3,
2375.
- Anderson A.C. and Smith S.C. (1973), J. Phys. Chem. Solids
34, 111.
- Archibald M.A.; Dunick J.E. and Jericho M.H. (1967),
Phys. Rev. 153, 786.
- Birch J.A.; Kemp W.R.G., Klemens P.G. and Tainsh R.J.
(1959), Aust. J. Phys. 12, 455.
- Blakemore J.S., Winstel J. and Edwards R.V. (1970),
Rev. Sci. Instr. 41, 835.
- Bleaney B. (1950), Proc. Roy. Soc. A204, 216.
- Brickwedde F.G., Van Dijk H., Durieux M., Clements J.R.
and Logan K. (1960), J. Res. NBS 64A, No. 1, 1.
- Carruthers P. (1961), Rev. Mod. Phys. 33, 92.
- Cooke A.H. (1949), Proc. Phys. Soc. A62, 269.
- Corak W.S., Garfunkel M.P., Satterhwaite C.B. and
Wexler A. (1955), Phys. Rev. 98, 1699.
- Daniels J.M. and Kurti N. (1954), Proc. Roy. Soc. A221,
243.
- Hansen M. (1958), Constitution of Binary Alloys (McGraw
Hill N.Y.).
- Harrison J.P. (1968), Rev. Sci. Instr. 39, 145.
- Jericho M.H. (1965), Phil. Trans. Roy. Soc. London 257,
385.

Johnson Matthey and Mallory, 110 Industry St., Toronto.

Gruner P. and Bross H. (1968), Phys. Rev. 172, 583.

Kemp W.R.G., Klemens P.G. and Tainsh R.J. (1957), Aust.

J. Phys. 10, 454.

Klemens P.G. (1958), in Solid State Physics Vol. 7,

edited by Seitz and Turnbull (Academic N.Y.).

Kronmüller H. (1972), Phys. Stat. Solidi(b) 52, 231.

Kusonoki M. and Suzuki H. (1969), J. Phys. Soc. Japan

26, 932.

Leaver A.D.W. and Charsley P. (1971), J. Phys. F1, 28.

Lindenfeld P. and Pennebaker W.B. (1962), Phys. Rev.

127, 1881.

Linz R.J., Chu T.K., Bouley A.C. and Lipschultz F.P.

(1974), Unpublished.

Mitchell M.A., Klemens P.G. and Reynolds C.A. (1971),

Phys. Rev. B3, 1119.

Moss M. (1967), J. of Appl. Phys. 36, 3308.

Morgan G.J. and Smith D. (1974), to be published.

Pearson W.B. (1958), A handbook of Lattice Spacings and

Structures of Metals and Alloys (Pergamon Press).

Pillinger W.L., Jastrum P.S. and Daunt D.G. (1958), Rev.

Sci. Instr. 35, 444.

Pippard A.B. (1957), J. Phys. Chem. Solids 3, 175.

Pohl, R.O. (1962), Phys. Rev. Letters 8, 481.

Rochlin G.I. (1970), Rev. Sci. Instr. 41, 73.

Saada G. (1966) in Theory of Crystal Defects, edited by

B. Gruber.

Seth R.S. and Woods S.B. (1970), Phys. Rev. B2, 2961.

Salter J.A.M., and Charsley P. (1967), Phys. Stat. Solidi
21, 357.

Schriempf J.T. (1967), Phys. Rev. Letters 19, 1131.

Schriempf J.T. (1968), Phys. Rev. Letters 20, 1034.

Sherman R.H., Sydoriak S.G. and Roberts T.R. (1964),
J. of Res. Nat. Bureau of Stds. Vol. 68A, #6,
579.

White G.K., Woods S.B. and Elford M.T. (1959), Phil. Mag.
4, 688.

White G.K. and Woods S.B. (1954), Phil. Mag. 45, 1343.

Windsor Metalcrystals Inc., P.O. Box 331, Westminster,
Md. 21157.

Zeller R.C. and Pohl R.O. (1971), Phys. Rev. B4, 2029.

Ziman J.M. (1958), Nuovo Cimento, Vol. 7, 353.

Ziman J.M. (1960), Electrons and Phonons (Oxford).

Zimmerman J.E. (1959), J. Phys. Chem. Solids 2, 299.

APPENDIX I

Description of a typical "RUN"

1. Solder probes on the specimen, measure the geometrical shape factor, then measure the resistance of the specimen immersed in a dewar of liquid helium.
2. Mount specimen in cryostat, attach thermometers, heater and electrical leads; check for continuity and accidental grounds.
3. Solder inner can and check for leaks using acetone. Then solder outer can and check for leaks using acetone.
4. Introduce exchange gas in rod space and specimen chamber at a pressure of several Torr.
5. Cool to nitrogen temperatures and check all electrical connections. Connect leak detector to specimen chamber.
6. Blow off liquid nitrogen by pressurizing dewar and transfer liquid helium.
7. When thermometers read 4 K fill the ^4He pot with liquid, taking care that the liquid is never cooled below its temperature in the dewar, and measure the electrical resistance of the specimen.
8. Pump exchange gas from specimen chamber using an oil diffusion pump till vacuum $\sim 2 \times 10^{-7}$ Torr. Pump for additional one hour and monitor sample space helium reading on leak detector.

9. Pump ^4He pot and take thermal conductivity points at intervals of 0.1 K as described earlier.
10. At 3 K condense ^3He in vapour pressure bulb.
11. At 2 K evacuate ^4He vapour pressure bulb and condense ^3He in pot.
12. Pump exchange gas from rod space and lift rod to isolate ^3He station from ^4He pot.
13. Pump on ^3He pot through needle valve, using a sealed Balzer's pump and take thermal conductivity points at intervals of 0.1 K down to 0.65 K. Check thermometer calibrations against vapour pressure between 0.7 to 2 K.
14. Using a mercury diffusion pump and bellows valve reduce temperature of ^3He pot and take thermal conductivity points until lowest temperature.
15. Using temperature controller heater boil off ^3He from pot and vapour pressure bulb.
16. Lower rod and introduce exchange gas in rod space and specimen chamber.
17. Remeasure electrical resistance of specimen.
18. Boil liquid helium from dewar and fill with liquid nitrogen.

APPENDIX II

ADDITIVITY OF THERMAL RESISTANCES

In Section 2.2.2, the total lattice thermal resistance was calculated by adding the thermal resistances W_{ge} (phonon-electron scattering) and W_{gd} (phonon-defect scattering). This procedure is valid only if the scattering processes have the same frequency dependence. If phonon-scattering processes with different frequency dependence are present simultaneously they must be combined by adding the appropriate reciprocal relaxation times before integrating over all frequencies. The relation to be used is then of the form:

$$\lambda_g = AT^3 \left[\left(\frac{1}{\tau_E} + \frac{1}{\tau_D} \right) \int_0^\infty \frac{x^4 e^{-x}}{(e^x - 1)^2} dx \right]$$

where $x = hv/kT$ and depends on fundamental constants and the velocity of sound. The relaxation times τ_E and τ_D are for phonon scattering by electrons and by defects respectively (Lindenfeld 1966).

Pippard (1957) has shown that for impure metals at low temperatures (when $q\lambda \sim 1$) the lattice conductivity does not follow a simple T^2 dependence but may be approximated by

$$\lambda_g = AT + BT^2$$

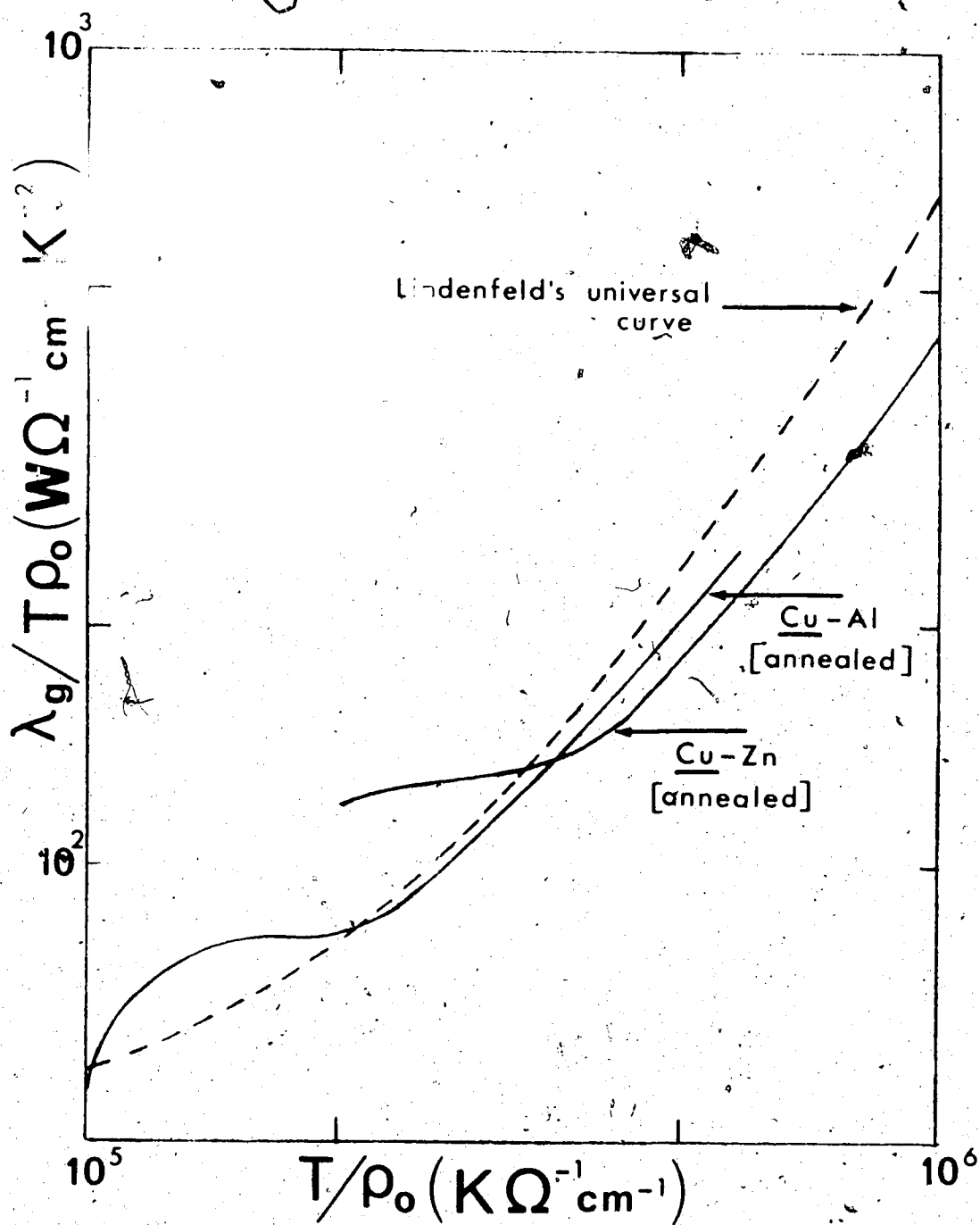


Fig. 13. $\lambda_g / T \rho_0$ vs T / ρ_0 .

Plotted on a universal curve (Fig. 13), λ_g should follow a T^2 dependence for large T/ρ_0 ($q \gg 1$) but change over to a linear temperature dependence for small values of T/ρ_0 ($q \ll 1$). Since all our measurements lie in the region where $q \ll 1$ it is important to see if the anomalies can be explained by the extra conductivity arising from the linear term.

Data for the annealed copper alloys are plotted in Fig. 13 as λ_g/T^2_0 vs T/T_0 . The dotted line represents the theoretical curve for copper as calculated by Lindenfeld (1962). In the region 1-4 K the data lie below the theoretical curve implying that some defect scattering still exists in the annealed specimens. At 1.2 K λ_g rises sharply above the theoretical limit which makes one conclude that the increase in λ_g cannot be explained by the "Pippard effect" in W_{ge} as the dotted line represents the limiting value for W_{ge} and yet the experimental results rise above it and the change in λ_g is too abrupt.

In the fully cold-worked alloy the arguments are unchanged even if W_{ge} and W_{gd} have different frequency dependence, because $W_{gd} \gg W_{ge}$ at all temperatures which is all that is necessary for our conclusions to follow.